PHILOSOPHICAL TRANSACTIONS OF THE ROYAL SOCIETY A MATHEMATICAL, PHYSICAL & ENGINEERING SCIENCES

On the Receptivity Problem for Gortler Vortices: Vortex Motions Induced by Wall Roughness

James P. Denier, Philip Hall and Sharon O. Seddougui

Phil. Trans. R. Soc. Lond. A 1991 **335**, 51-85
doi: 10.1098/rsta.1991.0036

On the receptivity problem for Görtler vortices: vortex motions induced by wall roughness

By James P. Denier[1], Philip Hall[1] and Sharon O. Seddougui[2]

[1]*Department of Mathematics, University of Exeter, North Park Road, Exeter, Devon EX4 4QE, U.K.*

[2]*I.C.A.S.E., MS 132C, NASA Langley Research Centre, Hampton, Virginia 23665, U.S.A.*

Contents

The receptivity problem for Görtler vortices induced by wall roughness is investigated. The roughness is modelled by small amplitude perturbations to the curved wall over which the flow takes place. The amplitude of these perturbations is taken to be sufficiently small for the induced Görtler vortices to be described by linear theory. The roughness is assumed to vary in the spanwise direction on the boundary-layer lengthscale, whilst in the flow direction the corresponding variation is on the lengthscale over which the wall curvature varies. In fact the latter condition can be relaxed to allow for a faster streamwise roughness variation so long as the variation does not become as fast as that in the spanwise direction. The function that describes the roughness is assumed to be such that its spanwise and streamwise dependences can be separated; this enables us to make progress by taking Fourier or Laplace transforms where appropriate. The cases of isolated and distributed roughness elements are investigated and the coupling coefficient which relates the amplitude of the forcing and the induced vortex amplitude is found asymptotically in the small wavelength limit. It is shown that this coefficient is exponentially small in the latter limit so that it is unlikely that this mode can be stimulated directly by wall roughness. The situation at $O(1)$ wavelengths is quite different and this is investigated numerically for different forcing functions. It is found that an isolated roughness element induces a vortex field which grows within a wedge at a finite distance downstream of the element. However, immediately downstream of the obstacle the disturbed flow produced by the element decays in amplitude. The receptivity problem at larger Görtler numbers appropriate to relatively large wall curvature is discussed in detail. It is found that the fastest growing linear mode of the Görtler instability equations has wavenumber proportional to the one-fifth power of the Görtler number. The mode can be related to both inviscid disturbances

Phil. Trans. R. Soc. Lond. A (1991) **335**, 51–85
Printed in Great Britain

and the disturbances appropriate to the right-hand branch of the neutral curve for Görtler vortices. The coupling coefficient between this, the fastest growing vortex, and the forcing function is found in closed form.

1. Introduction

Our concern is with the mechanism by which Görtler vortices in incompressible boundary layers are stimulated by wall roughness elements. We shall consider the cases of isolated and distributed roughness over the whole range of unstable Görtler numbers. In a recent paper (Hall 1990) the Görtler receptivity problem for free-stream disturbances was discussed; the present paper completes the discussion of the linear receptivity problem for Görtler vortices. However, some of the cases considered in this paper can be generalized to take account of finite amplitude effects but those situations will not be discussed here. Before discussing the receptivity problem in more detail we shall remind the reader of the main results of linear stability theory applied to boundary layers on curved walls. The paper mentioned above (Hall 1990) is for the most part a review of the linear and nonlinear stages of Görtler vortices so the reader is referred to that paper for a more detailed discussion of the various stages of Görtler vortex growth.

The main feature of Görtler vortices that makes them behave in a quite different manner than, for example, Tollmien–Schlichting waves or Rayleigh waves is that they are almost always dominated by non-parallel effects. This means that, at $O(1)$ wavenumbers and Görtler numbers, the concept of a unique neutral curve is not tenable; the position where a given vortex begins to grow is a function of its upstream history. Mathematically this property manifests itself through the parabolic nature of the disturbance equations for Görtler vortices. Thus Hall (1983) showed that at order one values of the Görtler number and wavenumber a small amplitude Görtler vortex is described by a parabolic system of equations, which in general must be solved numerically for each vortex wavenumber. The neutral curve corresponding to any fixed initial disturbance can be computed by marching the disturbance equations downstream, but it is a function of the initial disturbance.

The only exception to the situation discussed above is that when the vortex has a wavelength small compared with the boundary layer thickness. In this régime the vortex 'feels' the local structure of the boundary layer and is therefore able to develop in a quasi-parallel manner. Hall (1982*a*) showed that it is then possible to define a unique right-hand branch of the neutral curve which, at zeroth order, has the Görtler number proportional to the fourth power of the vortex wavenumber.

It had been assumed by authors previous to Hall (1982*a*) that Görtler vortices could be described in a self-consistent manner by making the parallel flow approximation and possibly appealing to, for example, the method of multiple scales to give the approximation some justification (see, for example, Floryan & Saric 1979). However, it is now accepted that no such justification can be made and that, if one is interested in the evolution of vortices with $O(1)$ wavelength in a boundary layer, the governing equations are indeed the parabolic equations solved by Hall (1983), thus no reduction to a set of ordinary differential equations is possible.

In the nonlinear régime the non-parallel characteristics of Görtler vortices are maintained and the disturbance equations must be solved numerically (Hall 1988). However, in the small wavelength nonlinear régime much analytical progress can be

PHILOSOPHICAL TRANSACTIONS OF THE ROYAL SOCIETY A MATHEMATICAL, PHYSICAL & ENGINEERING SCIENCES

made and it is possible to describe vortices so large that they have an $O(1)$ effect on the mean flow. Indeed in that régime it is found that the mean flow is actually driven by the vortices over most of the flow and adjusts itself so as to make all small wavelength vortices neutrally stable (see Hall & Lakin 1988). At even larger amplitudes the strongly nonlinear states described by Hall & Lakin (1988) become unstable to wavy vortex modes as discussed by Hall & Seddougui (1989).

The above description of Görtler vortex growth in the linear and nonlinear régimes also applies to compressible flows if the Mach number is not too large (Hall & Malik 1989; Wadey 1990). In the hypersonic limit Hall & Fu (1989, 1990) showed that the linear development of Görtler vortices becomes much simpler. In particular, for either a Sutherland or Chapman law fluid, the first term in the expansion of the neutral Görtler number in terms of Mach number and wavenumber is independent of non-parallel effects. That property remains true at higher order for a Chapman law fluid but, for a Sutherland law fluid, non-parallel effects dominate at second order.

The results discussed above are broadly in agreement with experimental observations, certainly the non-parallel incompressible calculations are much more in line with experimental observations than are the parallel flow calculations. However, the non-parallel theory causes philosophical problems for the transition prediction industry; the reason why this should be the case is obvious. Thus in, for example, the e^n rule for transition prediction it is necessary to know the unique growth rate for a vortex at a given downstream position, but the main result of the non-parallel work is that no such quantity exists. In the absence of a unique growth rate the method cannot be used so, in some cases, the outcome of the non-parallel work has been ignored and parallel flow theory used to predict the required unique growth rate. In fact an unstable Görtler vortex undergoes most of its linear growth at high wavenumbers so the latter type of calculation is not totally flawed. The point is, of course, that if the concept of a unique growth rate is tenable only at high wavenumbers, and as the growth rate can be found in a simple asymptotic manner there, the high wavenumber theory should be used to predict the growth rate there.

The motivation for much of the research in recent years on Görtler vortices has come from the Laminar Flow Control programme at NASA Langley. In particular, a type of wing cross-section developed there (see Harvey & Pride 1982) has significant regions of curvature on its underside. These concave sections are required to stabilize the attachment line and control flow separation but are possible causes of transition via the Görtler vortex mechanism. A question of some importance in the flow around this type of wing is to determine, given that curvature is required because of other considerations, how the curvature should be distributed to minimize the likelihood of transition induced by Görtler vortices. A matter of equal importance is that of whether changes to the curvature distribution made to suppress Görtler vortices will enhance the likelihood of transition being caused by other mechanisms. Further motivation to study compressible Görtler vortices comes from the necessity for engineers to understand the flow around turbine blades or the flow in engine inlets. In fact the stability problem associated with the latter flow is made much more difficult because of shock waves present in the flowfield, as yet no progress has been made with the Görtler vortex problem in the presence of shocks though some progress has been made with understanding the effect of shocks on travelling wave instabilities (Cowley & Hall 1990).

In the practical situations where the Görtler mechanism is thought to be important it remains an open question if free-stream disturbances or wall roughness

PHILOSOPHICAL TRANSACTIONS OF THE ROYAL SOCIETY A MATHEMATICAL, PHYSICAL & ENGINEERING SCIENCES

will cause the initial vortex growth. Without doubt in both the wind-tunnel and flight situations we can expect that streamwise vorticity impinging on the leading edge or generated by imperfections on the wing surface will be present. The main aim of the present paper is to determine the efficiency of surface imperfections in generating vortices. This will be done over the whole range of Görtler numbers, this means that we will have to discuss the spatial inviscid instability problem for Görtler vortices, apparently this has not been done previously.

We shall see that the investigations of Hall (1982*a*) at high Görtler numbers overlooked a wavenumber régime where the fastest growing spatial Görtler vortices occurs. A significant property of these modes is that they are wall modes, actually they are localized in an asymptotically thin layer at the wall. This distinguishes them from the neutral form of the small wavelength modes of Hall (1982*a*), which are trapped in a thin asymptotically small layer in the interior of the flow. The new modes which we describe are viscous but they connect in a simple way to the inviscid spatial modes in one limit, and with the neutral modes of Hall (1982*a*) in another limit. Because these most unstable modes choose to locate themselves at the wall, it turns out that they couple strongly with any forcing due to a surface imperfection. Our calculations suggest that the stimulation of these modes will be the most likely consequence of a quite general surface imperfection, therefore they are likely to be the source of transition in curved flows at high Görtler numbers. However, in addition to these modes, we shall discuss all other possible types of induced longitudinal vortex scalings. Our discussion applies to walls with small amplitude imperfections of somewhat arbitrary character but we concentrate mostly on the case when the perturbation is localized in the spanwise direction. For such walls we find that the vortices grow in a wedge shaped region downstream of the obstacle, though in the immediate downstream vicinity of the obstacle the disturbance decays.

The procedure adopted in the rest of this paper is as follows: in §2 we formulate the receptivity problem for Görtler vortices induced by surface imperfections. In §3 we consider the limiting form of this receptivity problem appropriate to the small wavelength limit; in this limit we are able to derive an asymptotic form for the coupling coefficient between the forcing and the induced vortex field. In §4 the $O(1)$ wavelength problem is investigated; here we allow the forcing to vary on a lengthscale comparable with, and shorter than, the boundary layer scale in the flow direction. In §5 we isolate the fastest growing mode of the Görtler stability equations. In §6 the receptivity problem for this mode is discussed; finally in §7 we draw some conclusions.

2. Formulation of the forced Görtler vortex problem

We consider the flow of a viscous fluid over a wall of variable curvature. We assume that L is a typical lengthscale over which the curvature changes. If U_∞ is a typical flow velocity a great distance from the wall, and ν is the kinematic viscosity, we define a Reynolds number, Re, by

$$Re = U_\infty L/\nu, \tag{2.1}$$

and we suppose that with respect to cartesian axes x^*, y^*, z^* the wall is defined by

$$y^* = L\{Re^{-\frac{1}{2}} g(x^*/L) + \Delta\, Re^{-\frac{1}{2}} f(x^*/L, Re^{\frac{1}{2}} z^*/L)\}, \tag{2.2}$$

where Δ is a small constant.

We define variables (x, y, z) by

$$(x, y, z) = (x^*, Re^{\frac{1}{2}}y^*, Re^{\frac{1}{2}}z^*)/L, \tag{2.3}$$

and a corresponding velocity vector by

$$(u^+, v^+, w^+) = (u^*, Re^{\frac{1}{2}}v^*, Re^{\frac{1}{2}}w^*)/U_\infty. \tag{2.4}$$

We restrict our attention to the limit $Re \to \infty$ and write

$$p^+ = \bar{p}(x) + \Delta\, Re^{-\frac{1}{2}}\tilde{p}(x, y, z) + O(\Delta^2), \tag{2.5a}$$

$$(u^+, v^+, w^+) = (\bar{u}, \bar{v}, 0) + \Delta(\tilde{u}, \tilde{v}, \tilde{w}) + O(\Delta^2), \tag{2.5b}$$

where p^+ is the pressure, scaled on ρU_∞^2, with ρ the fluid density. Moreover, $\bar{u}$ and $\bar{v}$ depend only on x and y, whilst $\tilde{u}, \tilde{v}, \tilde{w}$ depend on all three dimensionless coordinates. We first take the limit $\Delta \to 0$ with Re held fixed and equate terms of order Δ^0, Δ in the Navier–Stokes equations. In the resulting systems for $(\bar{u}, \bar{v}, 0, \bar{p})$ and $(\tilde{u}, \tilde{v}, \tilde{w}, \tilde{p})$ we take the further limit $Re \to \infty$ to obtain, at the zeroth order level of approximation in Re,

$$\left.\begin{aligned} \bar{u}_x + \bar{v}_y &= 0, \\ \bar{u}\bar{u}_x + \bar{v}\bar{u}_y &= -\bar{p}_x + \bar{u}_{yy}, \end{aligned}\right\} \tag{2.6}$$

and

$$\left.\begin{aligned} \tilde{u}_x + \tilde{v}_y + \tilde{w}_z &= 0, \\ \bar{u}\tilde{u}_x + \bar{v}\tilde{u}_y + \tilde{u}\bar{u}_x + \tilde{v}\bar{u}_y &= \Delta_2\,\tilde{u}, \\ \bar{u}\tilde{v}_x + \bar{v}\tilde{v}_y + \tilde{u}\bar{v}_x + \tilde{v}\bar{v}_y &= -\tilde{p}_y + \Delta_2\,\tilde{v}, \\ \bar{u}\tilde{w}_x + \bar{v}\tilde{w}_y &= -\tilde{p}_z + \Delta_2\,\tilde{w}. \end{aligned}\right\} \tag{2.7}$$

Here the operator Δ_2 is defined by

$$\Delta_2 = \partial_y^2 + \partial_z^2,$$

and by writing down a Taylor series expansion for the no-slip condition about $y = g$ we obtain the conditions

$$\bar{u} = \bar{v} = 0, \quad y = g(x), \tag{2.8a}$$

$$\tilde{u} = -f\bar{u}_y, \quad \tilde{v} = -f\bar{v}_y, \quad \tilde{w} = 0, \quad y = g(x). \tag{2.8b}$$

Meanwhile for large values of y we require that

$$\bar{u} \to u_e(x), \quad y \to \infty, \tag{2.9a}$$

$$(\tilde{u}, \tilde{v}, \tilde{w}) \to 0, \quad y \to \infty, \tag{2.9b}$$

where $u_e(x)$ is the dimensionless free-stream velocity; in this paper we shall confine our attention to Blasius flow so that $u_e = 1$. To bring out more clearly the destabilizing effect of wall curvature we make the Prandtl transformation

$$\begin{aligned} y &\to y - g, \\ \bar{v} &\to \bar{v} + g'\bar{u}, \\ \tilde{v} &\to \tilde{v} + g'\tilde{u}, \end{aligned}$$

whilst all other variables remain unchanged. In this case (2.6)–(2.9) become

$$\left.\begin{aligned} \bar{u}_x + \bar{v}_y = 0, \quad \bar{u}\bar{u}_x + \bar{v}\bar{u}_y &= -\bar{p}_x + \bar{u}_{yy}, \\ \bar{u} = \bar{v} = 0, \quad y = 0, \quad \bar{u} \to u_e(x), \quad y &\to \infty \end{aligned}\right\} \tag{2.10}$$

and

$$\left.\begin{aligned} \tilde{u}_x+\tilde{v}_y+\tilde{w}_z &= 0,\\ \bar{u}\tilde{u}_x+\bar{v}\tilde{u}_y+\tilde{v}\bar{u}_y+\tilde{u}\bar{u}_x &= \Delta_2\tilde{u},\\ \bar{u}\tilde{v}_x+\bar{v}\tilde{v}_y+\tilde{u}\bar{v}_x+\tilde{v}\bar{v}_y+G\chi(x)\,\bar{u}\tilde{u} &= -\tilde{p}_y+\Delta_2\tilde{v},\\ \bar{u}\tilde{w}_x+\bar{v}\tilde{w}_y &= -\tilde{p}_z+\Delta_2\tilde{w},\\ \tilde{u}=-f\bar{u}_y,\quad \tilde{v}=0,\quad \tilde{w}=0,\quad y &= 0,\\ \tilde{u},\tilde{v},\tilde{w}\to 0,\quad y\to\infty. & \end{aligned}\right\} \tag{2.11}$$

In (2.11) we have replaced $2\,\mathrm{d}^2g/\mathrm{d}x^2$ by $G\chi(x)$ where G and χ will be referred to as the Görtler number and wall curvature respectively. Thus (2.10) must first be solved for the basic state whilst (2.11) then determines the forced vortex flow. We further note that the wall condition on v could be modified so as to determine, for example, the effect of wall suction on the generation of vortices. Finally, in this section we assume that f may be written as

$$f=\tilde{f}(x)\,\tilde{q}(z)$$

so that (2.11) can be Fourier transformed in z to give

$$u_x+v_y+\mathrm{i}kw=0, \tag{2.12a}$$

$$\bar{u}u_x+\bar{v}u_y+v\bar{u}_y+u\bar{u}_x=u_{yy}-k^2u, \tag{2.12b}$$

$$\bar{u}v_x+\bar{v}v_y+v\bar{v}_y+u\bar{v}_x+G\chi\bar{u}u=-p_y+v_{yy}-k^2v, \tag{2.12c}$$

$$\bar{u}w_x+\bar{v}w_y=-\mathrm{i}kp+w_{yy}-k^2w, \tag{2.12d}$$

$$u=q(k)\,F(x),\quad v=0,\quad w=0,\quad y=0, \tag{2.12e}$$

$$u,v,w\to 0,\quad y\to\infty. \tag{2.12f}$$

Here k is the transform variable, $-q$ is the transform of $\tilde{q}$, u is the transform of $\tilde{u}$, etc., and we have defined $F(x)=\bar{u}_y(x,0)\tilde{f}(x)$. In the following sections we discuss the solutions of (2.12) in a variety of situations; for convenience we note that if p and w are eliminated from the disturbance equations we obtain

$$\begin{aligned} &\{\bar{u}_{xyy}+k^4+k^2\bar{v}_y\}\,v+\bar{v}_x\,u_{yy}+\{\bar{u}_{xxy}+k^2\bar{v}_x+k^2\chi G\bar{u}\}\,u\\ &\quad+\{\bar{u}_{yy}-\bar{u}\,\partial^2/\partial y^2+k^2\bar{u}\}\,v_x+2\{\bar{u}_{xy}+\bar{u}_x\,\partial/\partial y\}\,u_x\\ &\quad+v_{yyyy}-\bar{v}v_{yyy}-\{\bar{v}_y+2k^2\}\,v_{yy}+\{\bar{u}_{xy}+k^2\bar{v}\}\,v_y=0. \end{aligned} \tag{2.12g}$$

Thus the problem for the forced vortex flow can be reduced to the solution of (2.12b, g) subject to the boundary conditions (2.12e, f). At finite values of G the solution of this system can only be found by numerical integration. However it is first instructive to consider the receptivity problem for vortices with a wavelength appropriate to the right-hand branch of the neutral curve; the results we obtain are invaluable in interpreting the calculations at $O(1)$ wavelength which will be discussed in §4. Moreover the main result of the calculation is to show that the amplitude of a vortex trapped in a thin shear layer an order one distance from the boundary is an exponentially small fraction of the forcing amplitude at the wall. Essentially this is because the forcing decays away from the wall on a viscous lengthscale comparable with the vortex wavelength. However, the details of this decay are relevant to related receptivity problems where the mode of instability is concentrated away from the wall so we shall in the next section discuss the small wavelength limit in some detail. The related receptivity problems we alluded to above concern inviscid modes

of instability of compressible boundary layers, in particular the dominant small wavelength modes of hypersonic boundary layers (see, for example, Hall & Fu 1989, 1990; Cowley & Hall 1990).

3. The small wavelength limit

We now consider the asymptotic limit $k \to \infty$ in which case the unforced problem becomes unstable in a layer of thickness $k^{-\frac{1}{2}}$ located in a position which maximizes the downstream growth of the vortex. From Hall (1982*a*, *b*) we know that small wavelength vortices develop in a non-parallel manner in a k^{-1} neighbourhood of the neutral location. Thus, if the Görtler number G is written as

$$G = \tilde{G}k^4, \tag{3.1}$$

then suppose that, using the approach of Hall (1982*a*), we find that correct to zeroth order in k^{-1} the neutral location is given by $x = \bar{x}$. We then write

$$X = k(x - \bar{x}). \tag{3.2}$$

We will allow the wall forcing function $F(x)$ to be slightly more general than that assumed in §2; more precisely, we now allow F to vary on the X lengthscale so that

$$F(x) = \mathscr{F}(X). \tag{3.3}$$

We will now show how the wall roughness induces a longitudinal vortex structure within a k^{-1} neighbourhood of $x = \bar{x}$; notice that if we wish to recover the case with F varying on x lengthscale we simply need to replace $\mathscr{F}(X)$ by a constant in the following analysis.

It follows from (2.12) that viscous effects in the normal and spanwise directions are comparable when $\partial/\partial y \approx O(k)$; this is achieved in the bulk of the flow using a WKB type of expansion. However, as discussed by Hall (1982*a*), this expansion fails near the wall and where $\bar{u}\bar{u}_y$ has a local maximum. We suppose that this maximum occurs at $y = \bar{y}$ so that the forced flow must have a region II of depth $k^{-\frac{1}{2}}$ centred on $y = \bar{y}$. Above and below this region are two further regions, I and III, where the WKB structure is appropriate. At the bottom of region III the WKB structure will be seen to break down; in fact the six different WKB exponents collapse into just two distinct values as $y \to 0$. Thus an adjustment or transition layer is needed as $y \to 0$; we shall see below that this is of depth $k^{-\frac{3}{4}}$ and we refer to this region as IV. Finally, where $y = O(k^{-1})$, the viscous derivatives in the y direction again become important so that a wall layer, V, of depth k^{-1} is needed. The different regions are illustrated in figure 1.

The wall layer solution

Here we define ξ by

$$\xi = ky$$

and the wall conditions suggest that u and v are $O(1)$ here. In fact it can be seen from (2.12*a*) that if u is $O(1)$ in V then v must be of order k; we are therefore led to the expansion

$$u = u_0(\xi) + \ldots, \quad v = kv_0(\xi) + \ldots, \tag{3.4a, b}$$

and we expand the basic velocity component $\bar{u}$ in this layer as

$$\bar{u} = \lambda\xi k^{-1} + \ldots, \tag{3.5}$$

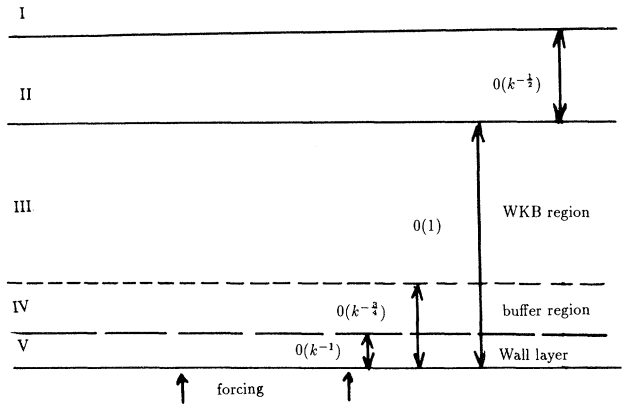

Figure 1. The different regions in the high wavenumber limit receptivity problem.

where $\lambda(\bar{x})$ is the wall shear at $x = \bar{x}$. A similar expansion can be written down for $\bar{v}$, but it is not needed here. If we substitute the above expansions into (2.12) we find that the zeroth order approximation to that system yields

$$\left.\begin{aligned} \{\mathrm{d}^2/\mathrm{d}\xi^2 - 1\}\, u_0 &= 0, \\ \{\mathrm{d}^2/\mathrm{d}\xi^2 - 1\}^2 v_0 &= -\bar{\chi}\tilde{G}\lambda\xi u_0, \\ u_0 = \mathscr{F}, \quad v_0 = v_{0\xi} &= 0, \quad \xi = 0, \end{aligned}\right\} \tag{3.6}$$

where $\bar{\chi} = \chi(\bar{x})$ and q has been set equal to 1. The solution of (3.6) which does not grow exponentially with ξ is then seen to be

$$u_0 = \mathscr{F}(X)\,\mathrm{e}^{-\xi}, \quad v_0 = -\bar{\chi}\tilde{G}\lambda\mathscr{F}\frac{\mathrm{e}^{-\xi}}{24}\{\xi^3 + 3\xi^2\}. \tag{3.7}$$

so that when $\xi \to \infty$ (3.7) gives

$$u \sim \mathscr{F}(x)\,\mathrm{e}^{-ky} + \ldots, \quad v \sim \frac{-\bar{\chi}\tilde{G}\lambda\mathscr{F}k^{\frac{7}{4}}}{24}(yk^{\frac{3}{4}})^3\,\mathrm{e}^{-ky} + \ldots. \tag{3.8}$$

Solution in IV

We can see from (3.8) that the next region, IV, is of depth $k^{-\frac{3}{4}}$ so we put

$$\eta = k^{\frac{3}{4}}y \tag{3.9}$$

and the appropriate expansions of u and v are then

$$u = U_0(\eta)\,\mathrm{e}^{-ky} + \ldots,$$
$$v = k^{\frac{7}{4}}V_0(\eta)\,\mathrm{e}^{-ky} + \ldots,$$

and after substituting into (2.12) and eliminating $V_0(\eta)$ from the resulting zeroth order equations we find

$$\left.\begin{aligned} \mathrm{d}^3U_0/\mathrm{d}\eta^3 - \tfrac{1}{8}\bar{\chi}\tilde{G}\lambda^2\eta U_0 &= 0, \\ U_0'(0) = U_0'' = 0, \quad U(0) &= \mathscr{F}(x). \end{aligned}\right\} \tag{3.10}$$

The solution of this system is

$$U_0 = \mathscr{F}\Psi(\sigma\eta) \tag{3.11}$$

where $\sigma = [\frac{1}{8}\bar{\chi}\tilde{G}\lambda^2]^{\frac{1}{4}}$ and Ψ satisfies

$$\mathrm{d}^3\Psi/\mathrm{d}\zeta^3 - \zeta\Psi = 0, \quad \Psi(0) = 1, \quad \Psi'(0) = \Psi''(0) = 0.$$

For large values of ζ the three possible forms for Ψ have

$$\Psi \sim \mathrm{e}^{\frac{3}{4}\zeta^{\frac{4}{3}}}, \quad \exp[\tfrac{3}{4}\mathrm{e}^{\pm\frac{2}{3}\pi\mathrm{i}}\zeta^{\frac{4}{3}}]$$

respectively so that Ψ grows exponentially when $\zeta \to \infty$. In fact the asymptotic form of Ψ for large ζ is found to be

$$\Psi \sim (\omega/\zeta^{\frac{1}{3}})\exp(\tfrac{3}{4}\zeta^{\frac{4}{3}}) + \ldots,$$

where ω is a constant given to three decimal places by $\omega = 0.285$.

It follows that for large values of η we can write u as

$$u \sim \frac{\omega 2^{\frac{1}{4}}\mathscr{F}(X)\exp[-ky + \frac{3}{4}\eta^{\frac{4}{3}}[\frac{1}{8}\bar{\chi}\tilde{G}\lambda^2]^{\frac{1}{3}}]}{k^{\frac{1}{4}}[\bar{\chi}\tilde{G}\lambda^2]^{\frac{1}{12}}y^{\frac{1}{3}}} + \ldots. \tag{3.12}$$

In fact the two other (complex) exponentially decaying solutions match onto exponentially decaying WKB solutions in III which do not have a turning point layer at $y = \bar{y}$. Thus it is sufficient for us to consider the matching of (3.12) with the WKB solution which does indeed have a turning point layer at $y = \bar{y}$; it is, of course, the part of the velocity field which drives the potentially unstable vortex velocity field.

The WKB solution in III

In this region we seek asymptotic solutions for u and v which take the form

$$(u, v) = \exp\left[k\int_0^y \theta(y)\,\mathrm{d}y\right]\{(u_0, k^2 v_0) + \ldots\}. \tag{3.13}$$

Here $\theta(y)$ is the WKB phase function and the relative scalings of u and v follow from the requirement that $\{\partial_y^2 + \partial_z^2\}U \sim V\bar{u}_y$ in III; the latter balance is the crucial one shown by Hall (1982*a*) to be necessary for small wavelength vortices. It is a routine matter to substitute for (u, v) from (3.13) into (2.12) and solve for (u_0, v_0). In fact at zeroth order u_0 and v_0 are not determined but the consistency of a pair of linear equations for these functions yields the phase equation

$$(\theta^2 - 1)^3 = -\tilde{G}\bar{\chi}\bar{u}\bar{u}_y,$$

where $\bar{u}(y) = \bar{u}(\bar{x}, y)$. So that u and v decay with y we must reject values of θ with positive real part. The three acceptable solutions are then found to be

$$\theta = -[1 - (\tilde{G}\bar{\chi}\bar{u}\bar{u}_y)^{\frac{1}{3}}]^{\frac{1}{2}}, \quad \theta = -[1 - (\tilde{G}\bar{\chi}\bar{u}\bar{u}_y)^{\frac{1}{3}}\mathrm{e}^{\pm 2\pi\mathrm{i}/3}]^{\frac{1}{2}}, \tag{3.14a, b}$$

where the branch of the square root in the right-hand half plane is to be taken. The first of these roots vanishes where $1 = \tilde{G}\bar{\chi}\bar{u}\bar{u}_y$ and this necessitates the existence of the turning point layer II. The complex roots lead to no such turning point layer so that the part of the WKB solution appropriate to these roots is valid in $0 < y < \infty$. In fact these solutions match directly onto the part of the solution in III appropriate to the complex valued large ζ solutions of (3.12). Thus we neglect this part of the WKB solution since it does not interact in any way with the induced vortex instability which we will calculate in II. We therefore write u in III as

$$u = \exp\left[-k\int_0^y [1 - \{\tilde{G}\bar{\chi}\bar{u}\bar{u}_y\}^{\frac{1}{3}}]^{\frac{1}{2}}\,\mathrm{d}y\right]\{u_0 + \ldots\} + \text{E.D.},$$

where E.D. denotes the other WKB solutions not having a turning point layer at $y = \bar{y}$. At higher order the amplitude function $u_0(X, y)$ is found to satisfy

$$-[\theta^2-1]\,\tilde{G}X\in(y)\,u_0-2\tilde{G}\bar{u}\bar{u}_y\,\bar{\chi}\bar{v}\theta u_0-2\tilde{G}\bar{\chi}\bar{u}^2\bar{u}_y\,u_{0_X}$$
$$+6\theta\tilde{G}\bar{\chi}\bar{u}\bar{u}_y\,u_{0_y}+3\theta'(\theta^2-1)^2(1-5\theta^2)\,u_0-4\theta\bar{\chi}\tilde{G}\bar{u}\bar{u}_{yy}\,u_0=0. \quad (3.15)$$

Here $$\in(y)=[\bar{u}\bar{u}_y\,\chi]_x|_{x=\bar{x}},$$

and $\bar{v}=\bar{v}(\bar{x},y)$. Thus u_0 satisfies a partial differential equation with coefficients dependent on both X and y. Non-parallel effects lead directly to the term proportional to X in (3.15). Furthermore, to match with the solution in IV we require

$$u_0\sim\frac{2^{\frac{1}{4}}\omega}{k^{\frac{1}{4}}[\bar{\chi}\tilde{G}\lambda^2]^{\frac{1}{12}}}\mathscr{F}(x),\quad y\to 0. \quad (3.16)$$

To simplify the solution of the equations for u_0 we write

$$u_0=\frac{2^{\frac{1}{4}}\omega(\bar{u}_y)^{\frac{2}{3}}U_0}{k^{\frac{1}{4}}[\bar{\chi}\tilde{G}\lambda^2]^{\frac{1}{12}}}|\theta|^{-\frac{1}{2}}|\theta^2-1|^{-1}\exp\{\Sigma(x,y)\}, \quad (3.17)$$

where

$$\Sigma=\frac{1}{3}\int_0^y\bar{v}\,\mathrm{d}y+\gamma X^2+\int_0^y\frac{\bar{u}}{3\theta}\left[\int_0^y\frac{N(y)}{6\theta}\,\mathrm{d}y\right]\mathrm{d}y+X\int_0^y\frac{N(y)}{6\theta}\,\mathrm{d}y, \quad (3.18)$$

with $$\gamma=\bar{\chi}^{-1}\{[\bar{u}\bar{u}_y\,\chi]_x/4\bar{u}^2\bar{u}_y\}|_{x=\bar{x},\,y=\bar{y}}, \quad (3.19)$$

and $$N(y)=(\bar{\chi}\bar{u}\bar{u}_y)^{-1}\{(\theta^2-1)(\chi\bar{u}\bar{u}_y)_x|_{x=\bar{x}}+4\bar{u}^2\bar{u}_y\,\bar{\chi}\gamma\}. \quad (3.20)$$

We note at this stage that $N(\bar{y})=0$ so that the integral

$$\int_0^y\frac{N(y)}{6\theta}\,\mathrm{d}y$$

converges when $y=\bar{y}$, even though $\theta(\bar{y})=0$. After writing u_0 in the form (3.17) we find that $U_0(x,y)$ satisfies

$$\partial U_0/\partial y-(\bar{u}/3\theta)\,\partial U_0/\partial X=0,\quad U_0=\mathrm{e}^{-\gamma X^2}\mathscr{F}(X),\quad y=0. \quad (3.21)$$

This system is most easily solved by taking the Laplace transform of U_0. However, before taking this transform it is convenient to suppose that $\mathscr{F}(X)=0$ for $X<X^*$ and that $u=v=0$ for $X<X^*$. We now make the change of variable $\tilde{X}=X-X^*$ and let $\hat{U}_0(s,y)$ be the transform of U_0. We then find that

$$\hat{U}_0=\bar{f}(s)\exp\left[s\int_0^y\frac{\bar{u}}{3\theta}\,\mathrm{d}y\right] \quad (3.22)$$

where $$\bar{f}(s)=\int_0^\infty\exp[-s\tilde{X}-\gamma(\tilde{X}+X^*)^2]\,\mathscr{F}(\tilde{X}+X^*)\,\mathrm{d}\tilde{X}. \quad (3.23)$$

We must now find the limiting form of the WKB solution when $y\to\bar{y}$; this will provide us with the required matching condition which we need to find the forced motion in II.

First, we note that when $y\to\bar{y}$ the phase function θ may be written as

$$\theta\sim-\tfrac{1}{2}M(\bar{y}-y)+\ldots, \quad (3.24)$$

where $$M^2 = \tfrac{1}{3}\bar{\chi}\tilde{G}[(-\bar{u}^2)_{yyy}]^*, \tag{3.25}$$

and a * denotes a function evaluated at $x = \bar{x}, y = \bar{y}$. It follows that in the limit $y \to \bar{y}$

$$\frac{u}{U_0} \sim \frac{A}{k^{\frac{1}{4}}}|y-\bar{y}|^{\frac{2\bar{u}^*_m I}{3M}-\frac{1}{2}} \exp\left\{XI+\gamma X^2+k\int_0^{\bar{y}}\theta\,\mathrm{d}y+\frac{k(y-\bar{y})^2}{4}M\right\}, \tag{3.26}$$

with $$A = \frac{2^{\frac{3}{4}}(\bar{u}^*_y)^{\frac{2}{3}}\exp\left\{\frac{1}{3}\int_0^{\bar{y}}\bar{v}\,\mathrm{d}y+\oint_0^{\bar{y}}\frac{\bar{u}}{3\theta}\left(\int_0^y\frac{N\,\mathrm{d}y}{6\theta}\right)\mathrm{d}y\right\}}{M^{\frac{1}{2}}[\bar{\chi}\tilde{G}\lambda^2]^{\frac{1}{12}}}, \tag{3.27}$$

and $$I = \int_0^{\bar{y}}\frac{N(y)}{6\theta}\,\mathrm{d}y.$$

Here $\oint$ denotes the finite part of an integral. Finally, we note that $\hat{U}_0$ in the limit $y \to \bar{y}$ takes the form

$$\hat{U}_0 \sim \bar{f}(s)|y-\bar{y}|^{\frac{2s\bar{u}_*}{3M}}\mathrm{e}^{s\Phi}, \tag{3.28}$$

where $$\Phi = \int_0^{\bar{y}}\frac{\bar{u}}{3\theta}\,\mathrm{d}y. \tag{3.29}$$

Solution in the transition layer

Here the solution is essentially that found by Hall (1982*a*, *b*) so that we only summarize briefly how it is obtained from the disturbance equations. The layer is of depth $k^{-\frac{1}{2}}$ so we define Y by

$$Y = k^{\frac{1}{2}}\{y-\bar{y}\}$$

and then u and v expand as

$$u = \bar{U}_0(Y)+k^{-\frac{1}{2}}\bar{U}_1(Y)+\ldots,$$
$$v = k^2\bar{V}_0(Y)+k^{\frac{3}{2}}\bar{V}_1(Y)+\ldots.$$

At zeroth order we obtain the equations

$$\bar{U}_0+\bar{V}_0\,\bar{u}^*_y = 0, \quad \tilde{V}_0+\bar{\chi}\tilde{G}\bar{u}^*\bar{U}_0 = 0,$$

which have a consistent solution if

$$\bar{\chi}\tilde{G}\bar{u}^*\bar{u}^*_y = 1.$$

Thus at zeroth order the leading order disturbance velocity field remains unknown. In fact, since $\bar{y}$ was chosen such that $(\bar{u}^2)_{yy}$ vanishes at $y = \bar{y}$ we must proceed to the $O(k^{-1})$ approximation level to the disturbance equations before $\bar{U}_0$ and $\bar{V}_0$ are found. At that order we find that $\bar{U}_0$ satisfies

$$\frac{\partial^2\bar{U}_0}{\partial Y^2}-\frac{2\bar{u}^*}{3}\frac{\partial\bar{U}_0}{\partial X}+\tfrac{1}{3}X\{\chi\tilde{G}\bar{u}\bar{u}_y\}^*_x\,\bar{U}_0-\tfrac{1}{4}M^2Y^2\bar{U}_0 = 0. \tag{3.30}$$

In the absence of any forcing we would seek solutions of this evolution equation which have $\bar{U}_0 \to 0, |Y| \to \infty$. However, for the forced problem we replace the condition at $Y = -\infty$ by one which enables us to match with the solution in III. With that in mind we take out the X dependence of $\bar{U}_0$ appropriate to (3.26) by writing

$$\bar{U}_0 = \mathscr{U}_0(X, Y)\,\mathrm{e}^{XI+\gamma X^2}$$

PHILOSOPHICAL TRANSACTIONS OF THE ROYAL SOCIETY A MATHEMATICAL, PHYSICAL & ENGINEERING SCIENCES

in which case $\mathscr{U}_0$ satisfies

$$\frac{\partial^2 \mathscr{U}_0}{\partial Y^2} - \tfrac{2}{3}\bar{u}^* \frac{\partial \mathscr{U}_0}{\partial X} - \tfrac{1}{4}M^2 Y^2 \mathscr{U}_0 - \tfrac{2}{3}\bar{u}^* I \mathscr{U}_0 = 0.$$

We can then make the change of variable $\tilde{X} = X - X^*$ and take the Laplace transform of this equation with respect to $\tilde{X}$. If we denote the Laplace transform of $\mathscr{U}_0$ by $\hat{\mathscr{U}}_0$ we find that $\hat{\mathscr{U}}_0$ satisfies a parabolic cylinder equation. More precisely, if $\hat{\mathscr{U}}_0$ is to vanish when $Y \to \infty$, we require that

$$\hat{\mathscr{U}}_0 = BU(2\bar{u}^*(s+I)/3M, M^{\frac{1}{2}}Y), \tag{3.31}$$

where $U(a, x)$ is a parabolic cylinder function. At this stage if s is chosen such that

$$2\bar{u}^*[s+I]/3M = -n - \tfrac{1}{2}$$

then $\hat{\mathscr{U}}_0(\pm\infty) = 0$. This choice of s corresponds to the linear eigensolutions found by Hall (1982*a*, *b*). In order to match the forced solution with that in III we note that when $Y \to -\infty$

$$\hat{\mathscr{U}}_0 \sim \frac{B\sqrt{(2\pi)}}{\Gamma(2\bar{u}^*[s+I]/3M + \frac{1}{2})} \mathrm{e}^{\frac{1}{4}Y^2} |Y|^{\frac{2\bar{u}^*}{3M}(s+I)-\frac{1}{2}} + \ldots.$$

Thus matching with the coreflow is achieved by choosing $B = B(s)$ such that

$$B\sqrt{(2\pi)}\, k^{\frac{1}{2}[\frac{2\bar{u}^*}{3M}(s+I)-\frac{1}{2}]} / \Gamma(2\bar{u}^*[s+I]/3M + \tfrac{1}{2})$$
$$= 2^{\frac{3}{4}} \bar{u}_y^{*\frac{2}{3}} \bar{f} \exp\left\{ \int_0^{\bar{y}} \theta \, \mathrm{d}y + \frac{1}{3}\int_0^{\bar{y}} \bar{v} \, \mathrm{d}y + \int_0^{\bar{y}} \frac{\bar{u}}{3\theta}\left[\int_0^y \frac{N}{6\theta} \mathrm{d}y \right] \mathrm{d}y \right\} \Big/ k^{\frac{1}{4}} M^{\frac{1}{2}} [\bar{\chi}\tilde{G}\lambda^2]^{\frac{1}{12}}.$$

Having determined B we can write down the inverse transform for $\mathscr{U}_0$ and the flow in II is then completely known. However, the gamma function has a sequence of poles at the origin and on the negative real axis so that, if $\bar{f}$ has no poles or branch cuts $\mathscr{U}_0$ will be found from the contribution of these poles. The least stable mode corresponds to the pole at the origin so that for large $\tilde{X}$ the solution will be dominated by that mode. As a measure of the size of the disturbance in the layer III we can take the centreline velocity. After some manipulation we see that the streamwise disturbance at $Y = 0$ for large values of X is given by

$$u \sim \frac{4.2^{-\frac{3}{4}} \bar{u}^{*-\frac{1}{3}} C \bar{f}[-I - 3M/4\bar{u}^*]\, k^{\frac{1}{4}}}{M^{\frac{1}{2}}[\bar{\chi}\tilde{G}\lambda^2]^{\frac{1}{12}}} \exp\{\gamma(X^* + \tilde{X})^2 + IX^* - 3\tilde{X}/4\bar{u}^*\}$$

where

$$C = \exp\left\{ k \int_0^{\bar{y}} \theta \, \mathrm{d}y + \frac{1}{3}\int_0^{\bar{y}} \bar{v} \, \mathrm{d}y + \int_0^{\bar{y}} \frac{\bar{u}}{3\theta}\left[\int_0^y \frac{N}{6\theta} \mathrm{d}u \right] \mathrm{d}y \right\}.$$

It follows from the above discussion that the coupling coefficient which relates a typical vortex velocity field with the forcing function is proportional to

$$k^{\frac{1}{4}} \exp\left\{ -k \int_0^{\bar{y}} |1 - \{\tilde{G}\bar{\chi}\bar{u}\bar{u}_y\}^{\frac{1}{3}}|^{\frac{1}{2}} \mathrm{d}y \right\}.$$

Thus, since this result is valid only in the limit $k \gg 1$ we see that small wavelength wall roughness is an extremely inefficient generator of Görtler vortices. The reason why this should be so is evident from the above discussion; it is, of course, a direct

consequence of the fact that the vorticity induced by the roughness must diffuse over an $O(1)$ distance to the layer where potentially unstable vortices of this wavelength can exist. We conclude that small wavelength vortices of wavenumber proportional to $G^{\frac{1}{4}}$ are almost certainly unlikely to be generated by wall roughness. Thus it would be extremely surprising if small wavelength vortices could be induced experimentally by wall roughness; however, the work of Hall (1990) shows that such vortices could be induced by free stream disturbances. We further note that, whatever the initial size of the vortex wavelength, the fact that it is observed experimentally that the vortex wavelength is conserved as it develops in the x direction means that ultimately the small wavelength limit becomes relevant. Now we shall relax the constraint on the size of the forced vortex wavelength and see if a stronger coupling between the induced form and the forcing is possible.

4. Vortices of $O(1)$ wavelength

Here we will be primarily interested in the case when the wavelength of the forced vortex is comparable with the boundary-layer thickness. We shall concern ourselves with both 'isolated' and 'distributed' roughness elements. For convenience we shall initially take $q = 1$ which corresponds to a delta function shaped hump in the spanwise direction, later we choose q to correspond to other shapes. Moreover, we shall also discuss the situation when the wall forcing function varies on a fast lengthscale, for an isolated roughness element this type of forcing provides unique initial conditions for the partial differential equations describing the vortex. Later in this section we shall return to the case when $F(x)$ varies on an $O(1)$ lengthscale, we shall see that this situation is the most efficient in producing linearly growing Görtler vortices of $O(1)$ wavelength.

We shall first determine solutions of (2.12) appropriate to the case when $F(x)$ varies on a relatively fast, $O(\epsilon)$, lengthscale. We suppose that the forcing begins at $x = \bar{x}$ and write

$$X = (x - \bar{x})/\epsilon$$

and then

$$F(x) = F^*(X). \tag{4.1}$$

In fact without any loss of generality we can take $\bar{x} = \frac{1}{2}$ so that the original lengthscale L has then been fixed in terms of the distance from the leading edge to the position where the forcing begins. Clearly we expect a different response of the flow when $\bar{x}$ is before or after the unstable régime of a vortex with wavenumber k; with $\bar{x}$ now fixed we must, of course, investigate that possibility by varying the Görtler number G.

To find the forced flow in a neighbourhood of $\bar{x}$ we first note that when $y \to 0$, $\bar{u}\,\partial_x \sim y/\epsilon$ so that convective and vertical diffusion effects are comparable in a layer of depth $\epsilon^{\frac{1}{3}}$, and the wall forcing implies that u will be $O(1)$ there. It follows that, if u is indeed $O(\epsilon^0)$ in this layer, then v will be $O(\epsilon^{-\frac{2}{3}})$ there. We deduce from (2.12c, d) that p and w must then be $O(\epsilon^{-\frac{5}{3}})$, $O(\epsilon^{-1})$ respectively. Thus if we put

$$\xi = y/\epsilon^{\frac{1}{3}}$$

then for $\xi = O(1)$ we seek a solution of (2.12) which takes the form

$$(u, v, w, p) = (u_0(X, \xi), \epsilon^{-\frac{2}{3}} v_0(X, \xi), \epsilon^{-1} w_0(X, \xi), \epsilon^{-\frac{5}{3}} p_0(X, \xi)) + \ldots,$$

whilst

$$(\bar{u}, \bar{v}) = (\epsilon^{\frac{1}{3}} \lambda \xi, \epsilon^{\frac{2}{3}} \mu \xi^2) + \ldots, \tag{4.2a, b}$$

where $\lambda = \bar{u}_y(\frac{1}{2}, 0), \mu = 2\bar{v}_{yy}(\frac{1}{2}, 0)$. If we substitute the above expansion into (2.12g) we find that

$$\left\{\frac{\mathrm{d}^2}{\mathrm{d}\xi^2} - \lambda s\xi\right\}\frac{\mathrm{d}^2\bar{v}_0}{\mathrm{d}\xi^2} = 0, \tag{4.3}$$

where s is the Laplace transform variable and $\bar{v}_0$ is the transform of v_0. If $\bar{v}_{0_\xi}$ is to be finite at infinity then

$$\frac{\mathrm{d}\bar{v}_0}{\mathrm{d}\xi} = A\int_0^\xi Ai(\lambda^{\frac{1}{3}}s^{\frac{1}{3}}\xi)\,\mathrm{d}\xi + B. \tag{4.4}$$

Here A and B are constants and Ai is the Airy function; however, the transformed continuity equation evaluated at the wall yields

$$B = -s\bar{F}(s). \tag{4.5}$$

Here $\bar{F}$ is the transform of F^* and $\bar{v}_{0_\xi}$ then vanishes at infinity if

$$A = -3s^{\frac{1}{3}}\lambda^{\frac{1}{3}}B. \tag{4.6}$$

Thus $\bar{v}_0$ can be written in the form

$$\bar{v}_0 = -s\bar{F}(s)\left\{\xi - 3\int_0^\xi \mathrm{d}\xi\left(\int_0^{(\lambda s)^{\frac{1}{3}}\xi} Ai(y)\,\mathrm{d}y\right)\right\}. \tag{4.7}$$

The transformed streamwise velocity component is then obtained from the x-momentum equation. We find that for large ξ, $\bar{u}_0$ and $\bar{v}_0$ have the asymptotic forms

$$\left.\begin{aligned}\bar{u}_0 &\sim -3\bar{F}s^{-\frac{1}{3}}\lambda^{-\frac{1}{3}}\omega\xi^{-1} + \ldots = -3\bar{F}s^{-\frac{1}{3}}\lambda^{-\frac{1}{3}}\epsilon^{\frac{1}{3}}y^{-1} + \ldots,\\ \bar{v}_0 &\sim 3\bar{F}s^{\frac{2}{3}}\lambda^{-\frac{1}{3}}\omega + \ldots,\end{aligned}\right\} \tag{4.8a, b}$$

where $\omega = \int_0^\infty \phi Ai(\phi)\,\mathrm{d}\phi$. Thus the flow in the wall layer induces a motion in the region where $y = O(1)$, the appropriate expansions there are

$$u = U_0\epsilon^{\frac{1}{3}} + \ldots, \quad v = V_0\epsilon^{-\frac{2}{3}} + \ldots \tag{4.9a, b}$$

and $\bar{U}_0, \bar{V}_0$, the transforms of U_0, V_0 are found to be given by

$$\bar{U}_0 = -(3\bar{F}\bar{u}'/\bar{u})\,s^{-\frac{1}{3}}\lambda^{-\frac{1}{3}}\omega q^*(y,k) + \ldots, \quad \bar{V}_0 = 3\bar{F}s^{\frac{2}{3}}\lambda^{-\frac{1}{3}}q^*(y,k)\,\omega + \ldots. \tag{4.10a, b}$$

Here q^* satisfies the stationary Rayleigh equation problem

$$\bar{u}(d_y^2 - k^2)\,q^* - \bar{u}''q^* = 0, \quad q^*(0) = 1, q^*(\infty) = 0. \tag{4.11}$$

Thus $\bar{U}_0$ and $\bar{V}_0$ decay to zero exponentially as $y \to \infty$ and satisfy the matching conditions (4.8). In each layer the transforms can be inverted and the large X form of this velocity field can be used as an initial condition for the full linearized disturbance equations. Now we consider the special case $F^* = \delta(X)$ where δ is the delta function. It is easy to show by inverting (4.7) and the corresponding form for $\tilde{u}_0$ that this choice of F^* leads to a similarity solution

$$u_0 \sim 1/X\tilde{\tilde{u}}_0(\xi/X^{\frac{1}{3}}), \quad v_0 \sim 1/X^{\frac{5}{3}}\tilde{\tilde{v}}_0(\xi/X^{\frac{1}{3}}).$$

In fact the above similarity solution is also the large X asymptotic form of a disturbance velocity field induced by a forcing function $F^*(X)$ of compact support. We conclude that the similarity solution can be used as the initial condition for the disturbance equations in the case when vortices are induced by an isolated roughness

element. We note here a related similarity solution situation arises in linear triple deck theory (Hunt 1971; Smith 1973), but here the absence of a streamwise pressure gradient in the Görtler equation causes the velocity field not to be confined to the wall layer. We will now show how the similarity solution can be derived directly from the disturbance equations.

The similarity solution

The appropriate similarity variable implied by the above discussion is

$$\zeta = y(\lambda/\tilde{x})^{\frac{1}{3}}, \tag{4.12}$$

where

$$\tilde{x} = x - \bar{x}, \tag{4.13}$$

and for $\zeta = O(1)$ the appropriate expansions for the disturbance velocity components u and v are expected to be

$$u = (\lambda^{\frac{1}{3}}/\tilde{x})\, u_0(\zeta) + \ldots, \quad v = (1/\tilde{x}^{\frac{5}{3}})\, v_0(\zeta) + \ldots.$$

The functions u_0 and v_0 are then found to satisfy

$$d_\zeta^2 u_0 + \tfrac{1}{3}\zeta^2 d_\zeta u_0 + \zeta u_0 = v_0, \quad d_\zeta^4 v_0 + \tfrac{1}{3}\zeta^2 d_\zeta^3 v_0 + \tfrac{7}{3}\zeta d_\zeta^2 v_0 = 0, \tag{4.14a, b}$$

together with the boundary conditions

$$u_0 = v_0 = d_\zeta v_0 = 0, \quad \zeta = 0.$$

After some manipulation it is possible to solve (4.14*b*) for $d_\zeta^2 v_0$ in terms of Whittaker functions. We can then show that there is a solution of (4.14*b*) which satisfies $v_0 = d_\zeta v_0 = 0, \zeta = 0$ and at infinity is such that $v_0 \sim 1 +$ exponentially small terms. Thus the solutions of (4.14*b*) which behave like ζ and ζ^{-5} when $\zeta \to \infty$ do not appear in the required solution for v_0; indeed if they were present we could not match the wall layer solutions valid in the region $y = O(1)$.

Having solved for v_0 we can then solve (4.14*a*) for u_0, however, at this stage we see that the homogeneous form of this equation has the eigensolution $u_0 = \zeta \exp(-\frac{1}{9}\zeta^3)$ so that the inhomogeneous equation can only be solved subject to $u_0 = 0, \zeta = 0$ if a finite multiple of the algebraically decaying solution $u_0 \sim \zeta^{-3}$ is retained. However, it is not possible to match that solution with the coreflow so we must choose $v_0 = 0$ or expand u and v in the form

$$u = (\lambda^{\frac{1}{3}}/\tilde{x})\, u_0(\zeta) + u_1(\zeta)/\tilde{x}^{\frac{7}{3}} + \ldots, \quad v = (1/\tilde{x}^{\frac{2}{3}})\, v_0(\zeta) + v_1(\zeta) + \ldots. \tag{4.15a, b}$$

In this case u_0 satisfies the homogeneous form of (4.14*a*) but v_0 satisfies an inhomogeneous form of (4.14*b*) with $\frac{7}{3}$ replaced by $\frac{4}{3}$. After some algebra we find that u_0 and v_0 are given by

$$(u_0, v_0) = (\zeta, -\zeta^2\lambda'/2\lambda^{\frac{4}{3}}) \exp(-\tfrac{1}{9}\zeta^3). \tag{4.16a, b}$$

The functions u_0, v_0 are shown in figure 2.

The result given in (4.16) is of some importance because it means that, at leading order in the expansions of u and v, the disturbed flow is confined to the wall layer. However, this is not the case at higher order. In fact we can show that u_1 is given by

$$u_1 = (-k^2/3\lambda^{\frac{2}{3}})\{e^{-\frac{1}{9}\zeta^3} - \hat{u}_1(\zeta)/\hat{u}_1(0)\}, \tag{4.17a}$$

where $\hat{u}_1$ is the exponentially decaying solution of

$$d_\zeta^2 \hat{u}_1 + \tfrac{1}{3}\zeta^2 d_\zeta \hat{u}_1 + \tfrac{1}{3}\zeta \hat{u}_1 = 0. \tag{4.17b}$$

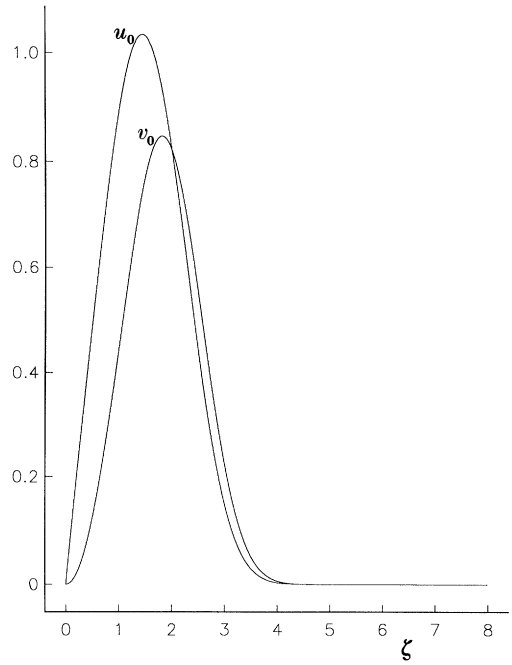

Figure 2. The similarity functions $u_0(\zeta), v_0(\zeta)$ given by (4.16) evaluated at $\bar{x} = 0.5$.

The function v_1 is found to satisfy

$$[d_\zeta^2 + \tfrac{1}{3}\zeta^2 d_\zeta + \tfrac{2}{3}\zeta]\, d_\zeta^2 v_1 = \frac{2\lambda'}{3\lambda^{\frac{4}{3}}}[1 + \zeta d_\zeta]^2 u_1 + \frac{k^2}{\lambda^{\frac{2}{3}}}[2d_\zeta^2 v_0 + \tfrac{1}{3}\zeta d_\zeta v_0 + \tfrac{2}{3}\zeta v_0], \qquad (4.17c)$$

which must be solved subject to $v_1 = v_1' = 0, \zeta = 0$ and

$$v_1 \sim \text{const.} + \text{exponentially small terms}, \quad \zeta \to \infty.$$

We found by integrating the above equation numerically that this constant is non-zero so the $y = O(1)$ region has a disturbance velocity field of the form

$$u \sim (-\tilde{x}\bar{u}'/\bar{u})\, q^*(y, k), \quad v \sim q^*(y, k), \qquad (4.18)$$

where q^* satisfies (4.11) so that $(u, v) \to 0$ when $y \to \infty$. In figure 3 we have shown the function $q^*(y, k)$ for several values of the wavenumber k. We note that for the smaller values of k the function q^* has a maximum value away from the origin. At larger values of k the function $q^* \sim \mathrm{e}^{-ky}$ and therefore decreases monotonically as y increases from zero. We can then combine (4.10), (4.15) to give a composite velocity field at some small value of $\tilde{x}$ which can be used as initial conditions for the full Görtler disturbance equations. Before discussing our numerical results obtained for such a calculation we note that the similarity solution obtained above is unique only up to a multiplicative constant. That constant can be evaluated for a particular wall forcing function by obtaining the large X form of the velocity field obtained by inverting the transformed velocity field. The constant will be $O(1)$ and is, of course, a function of the particular function chosen. Moreover, this 'coupling' constant gives a measure of the input disturbance velocity field for the marching problem. We see below that at the position where the downstream velocity field induced by this

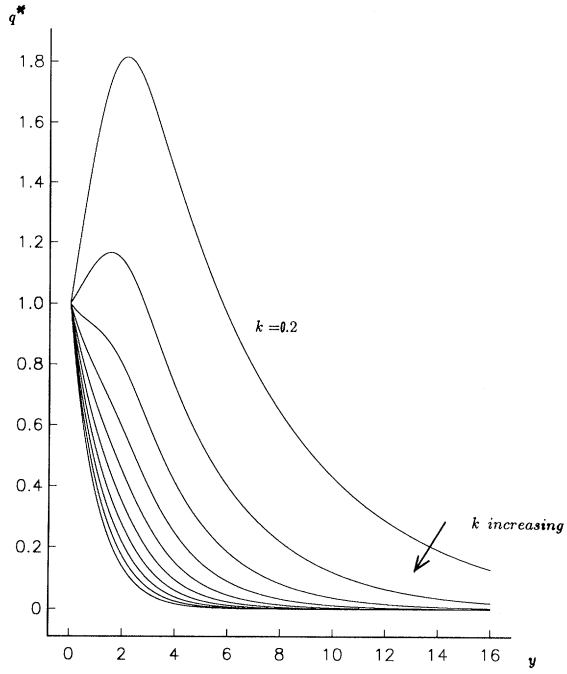

Figure 3. The solution of (4.11) for $k = 0.2, 0.3, \ldots, 1.1$.

disturbance begins to grow it has decreased in magnitude several orders of magnitude so that the boundary layer is extremely unreceptive to this type of forcing. For that reason it seems unnecessary for us to give values for the $O(1)$ coupling constant relating the forcing function and the similarity solution.

The numerical work

Now we shall report on some results we have obtained by integrating the Görtler vortex equations with the similarity solution discussed above used to provide an initial vortex velocity field. This solution was used to begin the calculations with $x = 0.5 + \Delta x$ for Δx small. The results presented here were obtained with $\Delta x = 0.004$, 1600 points in the y direction and a vertical step length equal to 0.02. The results were of course verified by varying these quantities in particular cases. It is of interest to note at this stage that the similarity solution (4.16) gives an initial vortex field with the u and v velocity components of the same sign (since λ' is negative). It is well known that Görtler vortices generally have these components of opposite sign when they are unstable so we might anticipate that localized roughness will not be a particularly efficient generator of this type of instability. The scheme used to march the Görtler equations downstream is precisely that used by Hall (1983) so we give no details of it here. As a measure of the disturbance energy we used $E(x)$ defined by

$$E = \int_0^\infty (u^2 + v^2 + w^2)\,\mathrm{d}y$$

and the local growth rate $\beta = E^{-1}\,\mathrm{d}E/\mathrm{d}x$. Following Hall (1983) the position of neutral stability can be defined as the location where $\beta = 0$. This position will to some extent depend on the choice of the flow property used to define β. Our calculations

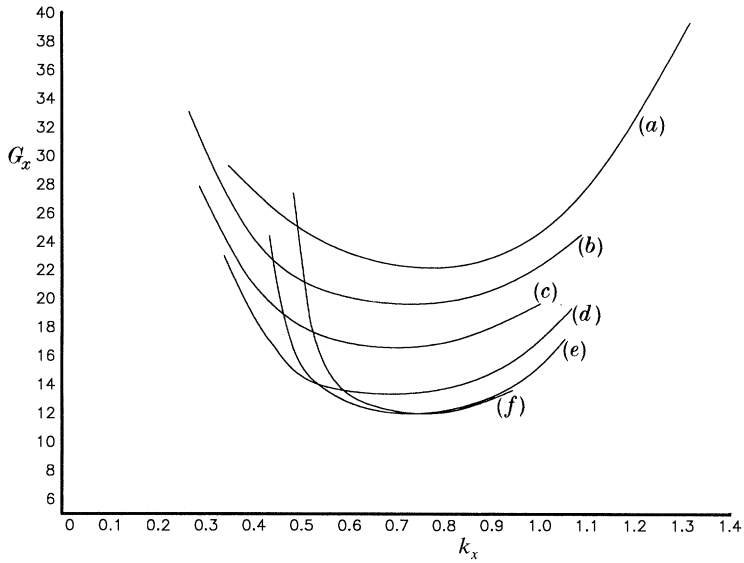

Figure 4. The neutral curves corresponding to an initial disturbance constructed from the similarity solution. $G = 20\,(a)$, $15\,(b)$, $10\,(c)$, $5(d)$, $2.5\,(e)$, $2\,(f)$.

for several values of k, G showed that E decreases by several orders of magnitude before β becomes positive. Effectively this means that the type of localized forcing discussed so far in this section will generate Görtler vortices but the vortices produced by the forcing are significantly reduced in size before they begin to grow. However, in the absence of any other forcing, this type of mechanism will be that responsible for the growth of vortices and so it is worth giving some more detailed results. For several values of k with fixed values of G we computed the position at which the induced vortex structure begins to grow. The local wavenumber and Görtler number were calculated at that point and used to generate a neutral curve in the local wavenumber (k_x), local Görtler number (G_x) plane. These curves are plotted in figure 4 for several values of G. It is important to realize at this stage that, since the forcing was imposed at the same value of x in each case, the value of G used is a measure of how close the forcing is to the unstable region. We see in figure 4 that the critical Görtler number for a given value of G initially decreases with G. However, the lowest critical Görtler number occurs when G is about 2 and then takes on a value of about 12. We conclude then that localized wall-roughness in its most dangerous form produces the growth of the vortex system when the local Görtler number is about 12. Here it is of interest to note that the corresponding critical Görtler number appropriate to free-stream disturbances is about 6 so that free-stream disturbances are the most dangerous. Indeed the energy loss of a vortex induced by a free-stream disturbance is only an $O(1)$ fraction of its initial value so it would appear that the localized wall roughness mechanism would be relevant only in an experimental facility with remarkably small free-stream disturbances.

In figure $5a, b$ we show the downstream development of the velocity field induced by a delta function disturbance imposed at $x = 0.5$ with $k = 0.4, G = 5$. We notice that the initial forms of the streamwise and normal disturbance velocity components are different than their ultimate unstable forms because they are of the same sign. This is possibly one of the reasons why localized wall roughness is not an efficient

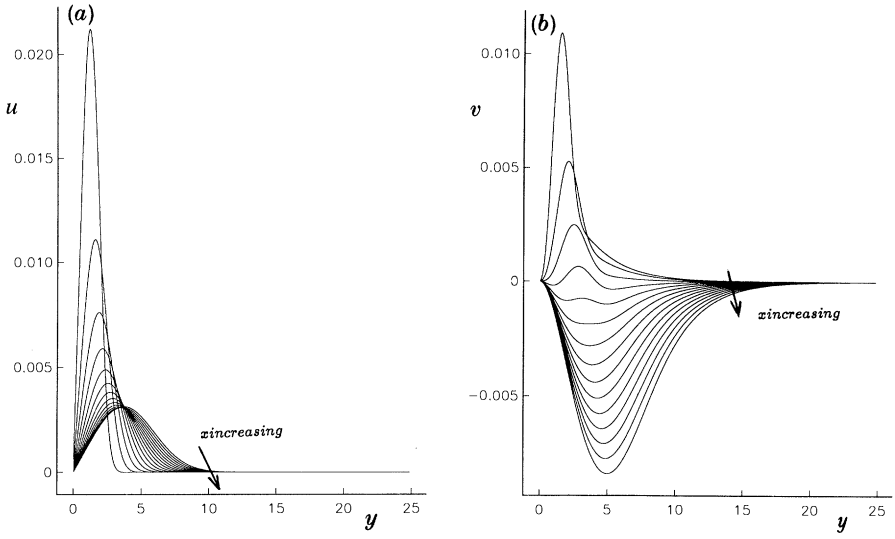

Figure 5. (*a*), (*b*) The downstream development of the velocity field induced by the similarity solution for the case $k = 0.4, G = 5$. The disturbance corresponds to a delta function forcing function at $x = 0.5$ and is shown at $x = 0.7, 0.9, \ldots, 3.5$.

generator of Görtler vortices. We further note that the velocity field at the larger values of x is quite typical of the non-parallel velocity fields obtained by Hall (1983). To quantify the inefficiency of localized wall roughness at generating Görtler vortices let us consider figure 5*b* in more detail. Since almost all of the energy of a vortex is in the streamwise velocity component we see in figure 5*b* that the energy of the vortex decreases by a factor of about 0.01 before it begins to grow. Thus we see that the amplitude of vortex when it begins to grow is about 0.1 of its initial value.

Now we shall discuss some solutions we have obtained for the forced vortex problem when the forcing occurs on an $O(1)$ streamwise lengthscale. The equations (2.12*b*, *g*) were solved using the approach of Hall (1983) subject to the conditions (2.12*e*, *f*). Here we shall report on calculations for the case when $F(x)$, the forcing function, is given by

$$F = 40(x-\tfrac{1}{2})\exp\left[-20(x-\tfrac{1}{2})^2\right], \quad x \geqslant \tfrac{1}{2}. \tag{4.19}$$

The disturbance equations for a given k were marched forward from $x = 0$ with zero initial disturbance. For a given function $q(k)$ we can invert the Fourier transform in z to give the velocity field induced by a hump of height proportional to $\tilde{q}(z)$, the inverse of $q(k)$. Before discussing our results we point out that further calculations for wall shapes other than (4.19) were carried out and gave qualitatively similar results.

In figure 6*a*, *b* we show the development of the functions u and v corresponding to the case (4.19) with $k = 0.45, G = 8$. We note that at smaller values of x the maximum of u occurs at the wall. We see that subsequently the maximum value of u occurs at a position which moves away from the wall and that the smallest maximum value occurs at about $x = 3.5$ and is approximately 0.26. This is to be compared with a maximum value of 4.84 of $F(x)$. Thus we now see that for a non-localized wall forcing there is a strong coupling between the induced vortex field and the forcing. Furthermore we point out that the ratio between the smallest maximum of u and the maximum of F is a function of k and G. Thus by 'tuning' k and G we

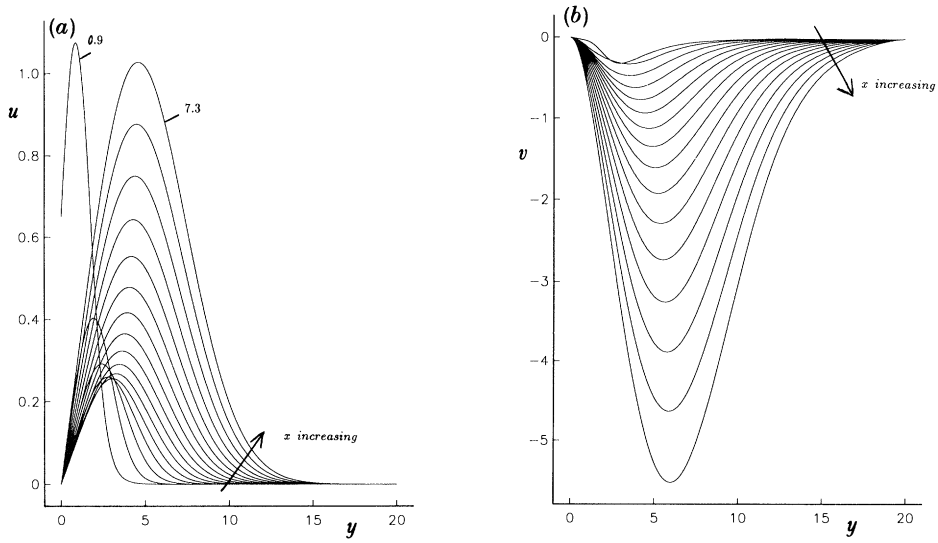

Figure 6. (*a*) The development of $u(x, y, k)$ corresponding to the forcing function (4.19) with $k = 0.45, G = 8$. (*b*) The development of $v(x, y, k)$ corresponding to the forcing function (4.19) with $k = 0.45, G = 8$. The profiles shown correspond to $x = 0.9, 1.3, \ldots, 7.3$.

can in principle maximize the coupling coefficient between the vortex field and the forcing. However, such a calculation was not carried out since it would require a great deal of computer time. Moreover, the results of figure 5*a*, *b* are sufficient for us to say that distributed forcing produces a strong coupling between the induced flow and the forcing. Perhaps this significant result has been appreciated for some time by experimentalists who have induced Görtler vortices by placing strips of tape on the wall of the test section of the experiment.

Now let us consider some results we have obtained for a wall with

$$\tilde{q}(z) = \tfrac{1}{4}\pi^{\frac{1}{2}} \mathrm{e}^{-\frac{1}{16}z^2}. \tag{4.20}$$

To monitor the strength of the induced vortex activity we computed $u^*(k, x, y)$, the maximum value of u, as a function of k, x and y, and the wall shear stress as a function of k. By inverting the transform in z numerically we were then able to obtain contours of u_M, the inverse of u^*, and the wall shear as functions of x and z. The results obtained for the two functions were similar so we shall concentrate on results for u_M. Figure 7*a–d* shows results obtained for u_M for the obstacle defined by (4.20). The results shown correspond to $G = 4$, 8, 12, 16. The size of G is a measure of how soon we expect vortices to grow; in the absence of a unique neutral curve for the Görtler problem we cannot be more precise than this. In the horizontal direction x varies from 0.7 to 9 whilst in the vertical direction z varies between $-20, 20$. We could have demonstrated the same effect shown in figure 7 by fixing G and varying the position where the forcing was switched on. Figure 7 shows clearly that immediately after the obstacle the disturbance velocity field decays initially and is concentrated in a wake behind the obstacle. Further downstream the curvature of the wall re-amplifies this disturbance field into Görtler vortices which spread out within a wedge-shaped region. The position where this amplification takes place is a function of G; as we would expect amplification of the vortices occurs closer to the obstacle as G is increased.

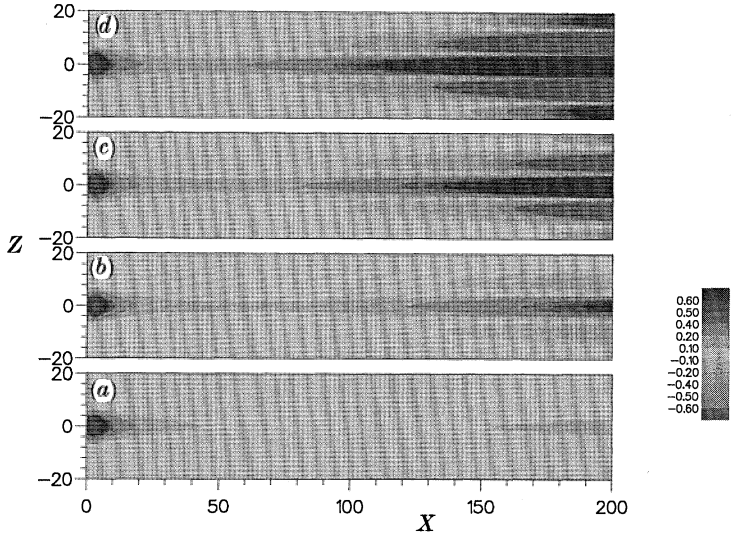

Figure 7. Contour plots of u_m in the xz plane for the obstacle defined by (4.20). The results correspond to (*a*) $G = 4$, (*b*) $G = 8$, (*c*) $G = 12$ and (*d*) $G = 16$.

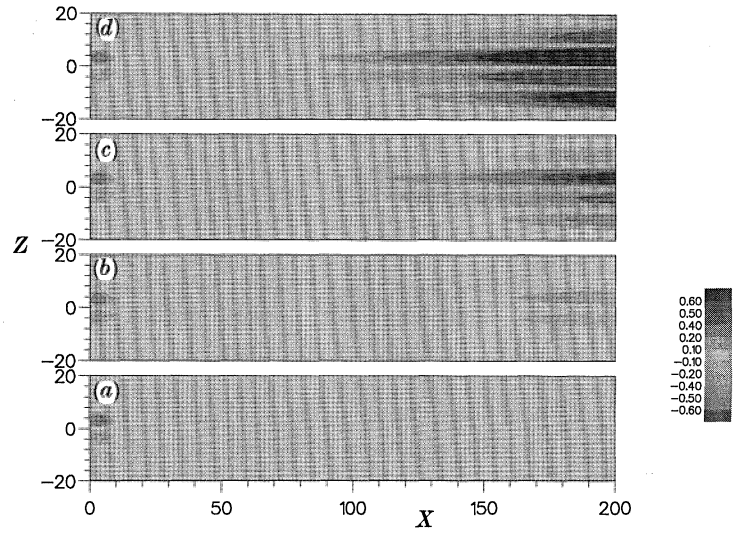

Figure 8. Contour plots of u_m in the xz plane for the obstacle defined by (4.21). The results correspond to (*a*) $G = 4$, (*b*) $G = 8$, (*c*) $G = 12$ and (*d*) $G = 16$.

Further calculations were carried out for asymmetric obstacles and in figure 8*a–d* we show results corresponding to figure 7 but with q now given by

$$\tilde{q} = \tfrac{1}{32}\pi^{\frac{1}{2}} z\, \mathrm{e}^{-\frac{1}{16}z^2}. \tag{4.21}$$

We see that the induced vortex field now is asymmetric about $z = 0$ but otherwise the vortex pattern is essentially the same as that computed for (4.20). Again we see a wake immediately behind the obstacle where the disturbance initially decays before being amplified into a Görtler vortex further downstream. The angle of the wedge within which the vortex activity becomes established for both the symmetric and

asymmetric obstacles is a function of the wall shape and the initial Görtler number. Because of the scalings used in the streamwise and spanwise directions the angle is typically of order $Re^{-\frac{1}{2}}$. However, from figures 7 and 8 it is clear that the angle increases with G. This is consistent with our physical intuition since we would expect that at higher Görtler numbers the vortex activity would spread out from the obstacle more rapidly. Other calculations which we carried out showed, not surprisingly, that the wedge angle increases as the spanwise extent of the obstacle grows. In an experiment the wall roughness would not be localized at one spanwise location so we would expect to see several wedges of vortex activity generated by the different roughness distributions merging into a uniform vortex field further downstream. We note that the onset of vortices in such wedge shaped regions has been observed experimentally by, for example, Mangalam *et al.* (1991). We conclude that a roughness element of lengthscale $O(L), O(Re^{-\frac{1}{2}}L)$ in the streamwise and spanwise directions respectively will produce an induced vortex field with an almost negligible drop in amplitude. Moreover, the onset of vortex activity will occur in a wedge-shaped region behind the obstacle.

In other experiments vortices have been generated by fixing strips of tape at periodic spanwise locations, if the spanwise spacing is chosen carefully then the induced vortex field observed in an experiment is found to have the same spanwise periodicity. The formulation of the receptivity problem discussed in this section could of course be used to describe that situation. However, it is clear that the induced vortex field must have a spanwise wavelength which depends on the rate of growth of the different modes. At finite Görtler numbers there is no such thing as a fastest growing mode so the wavelength selection problem can only be tackled by the type of numerical simulation discussed above. However, when the initial Görtler number of the flow is increased we might expect that the induced vortex field might have some unique structure associated with the right-hand branch of the neutral curve. The discussion of the previous section suggests that the small wavelength modes described by Hall (1982*a*) would have exponentially small amplitudes when induced by wall roughness so it is an open question as to what the induced vortex field would look like at large initial Görtler numbers. This question is also of some practical importance since it is relevant to the generation of vortices on turbine blades where the relatively large curvature of the blade means that the appropriate Görtler number is large. To answer this question it is necessary for us to look more carefully at the different vortex structures which are possible at high Görtler numbers, this matter is now addressed in the following section.

5. The most unstable Görtler vortex

We recall that the only part of the wavenumber–Görtler-number plane that can be described in a self-consistent manner by a parallel flow theory corresponds to large values of the Görtler number and wavenumber. More precisely we note that, in the limit $G \to \infty$ with $k \sim G^{\frac{1}{4}}$, neutral vortices described by the asymptotic structure of Hall (1982*a*) exist. Moreover, in the neighbourhood of the neutral state spatially amplified modes with growth rates $O(k^2)$ occur. These modes develop in the streamwise direction in such a way as to maximize their local growth rate. To isolate the fastest growing mode at high Görtler number (note that this concept is not tenable at finite Görtler numbers) we investigate the wavenumber spectrum close to the right-hand branch of the neutral curve. The analysis is based almost entirely on

that given by Hall (1982*a*), so we give only the most relevant results here; in fact the analysis of §3 essentially outlines the neutral structure of such modes if the forcing is switched off.

Consider then the solution of (2.12*b*, *g*) in the limit $G \to \infty$ with $k = O(G^{\frac{1}{4}})$. More precisely we write

$$k = \lambda G^{\frac{1}{4}}, \tag{5.1}$$

where $\lambda = O(1)$ initially but later it will be informative to move further away from the right-hand branch by letting $\lambda \to 0$. We seek a solution of (2.12*b*, *g*) in a layer of depth $k^{-\frac{1}{2}} \sim G^{-\frac{1}{8}}$ centred on the location

$$y = \bar{y}(x).$$

The appropriate expansion of the disturbance velocity u there is

$$u = \exp\left[G^{\frac{1}{2}} \int^x \beta(x)\,\mathrm{d}x\right]\{u_0(\psi, x) + k^{-\frac{1}{2}} u_1(\psi, x) + \ldots\} \tag{5.2}$$

together with a similar expansion for $k^{-2}v$; here $\psi = \lambda^{\frac{1}{2}} G^{\frac{1}{8}}\{y - \bar{y}\}$ and we have anticipated a growth rate of size $O(G^{\frac{1}{2}})$. In the layer of vortex activity we write

$$\bar{u} = \bar{u}_0(x) + \lambda^{-\frac{1}{2}} \bar{u}_1(x)\,\psi G^{-\frac{1}{8}} + \ldots \tag{5.3}$$

and, following Hall (1982*a*), we find that the zeroth order approximation to the eigenrelation is

$$\{\bar{u}_0 \beta + \lambda^2\}^2 = \chi \bar{u}_0(x)\,\bar{u}_1(x). \tag{5.4}$$

At this stage $\bar{y}(x)$ has not been fixed so we must interpret (5.4) as an equation to determine $\beta = \beta(\lambda, x, \bar{y}(x))$. If there is no forcing the vortex must decay exponentially as $|\psi| \to \infty$, this provides a second condition

$$(\partial/\partial y)[(\bar{u}(x, y)\,\beta + \lambda^2)^2 - \chi \bar{u}(x, y)\,\bar{u}_y(x, y)]|_{y=\bar{y}} = 0. \tag{5.5}$$

The vertical structure of the vortex is then obtained in terms of parabolic cylinder functions as was found in §3. We can then eliminate the dependence of β on $\bar{y}$ by combining (5.4) and (5.5) to give $\beta = \beta(\lambda, x)$. We note that the vortices are responding in a quasi-parallel manner so we could in fact scale x out of the problem by redefining λ and β. In particular if $\bar{u}$ corresponds to a Blasius boundary layer so that $\bar{u} = f'(\eta) = f'(y/\sqrt{(2x)})$, where f is the Blasius function then we must write $\beta = (\chi/\sqrt{(2x)})^{\frac{1}{2}}\beta^\dagger$, $\lambda = (\chi/\sqrt{(2x)})^{\frac{1}{4}}\lambda^\dagger$, in which case the simplified problem for $\beta^\dagger(\lambda^\dagger)$ is

$$(f'\beta^\dagger + \lambda^{\dagger 2})^2 = f'f'', \quad 2f''\beta^\dagger(f'\beta^\dagger + \lambda^{\dagger 2}) = (f'f'')', \tag{5.6a, b}$$

where the Blasius function is to be evaluated at some $\eta = \eta^\dagger$ where (5.6*b*) holds. In figure 9*a*, *b* we show $\beta^\dagger$ and $\eta^\dagger$ as functions of $\lambda^\dagger$. The cut-off value of $\eta^\dagger \sim 1.5$ corresponds to the neutral state found by Hall (1982*a*). However, we see that $\beta^\dagger$ is a monotonic decreasing function of $\lambda^\dagger$ and in fact has a singularity when $\lambda^\dagger \to 0_+$. An analysis of (5.6*a*, *b*) shows that in that limit

$$\beta^\dagger \sim \lambda^{\dagger -2}, \tag{5.6c}$$

so that small wavelength vortices become progressively more unstable as $k/G^{\frac{1}{4}} \to 0$. Thus we reach the conclusion that the quasi-parallel approach of Hall (1982*a*) does not capture the fastest growing mode and that the most unstable modes are probably to be found concentrated in a layer approaching the wall. Interestingly it is found that the fastest growing temporal mode is captured by the asymptotic structure of Hall (1982*a*); unfortunately the temporal modes are irrelevant to the receptivity problem for free-stream or wall induced vortices.

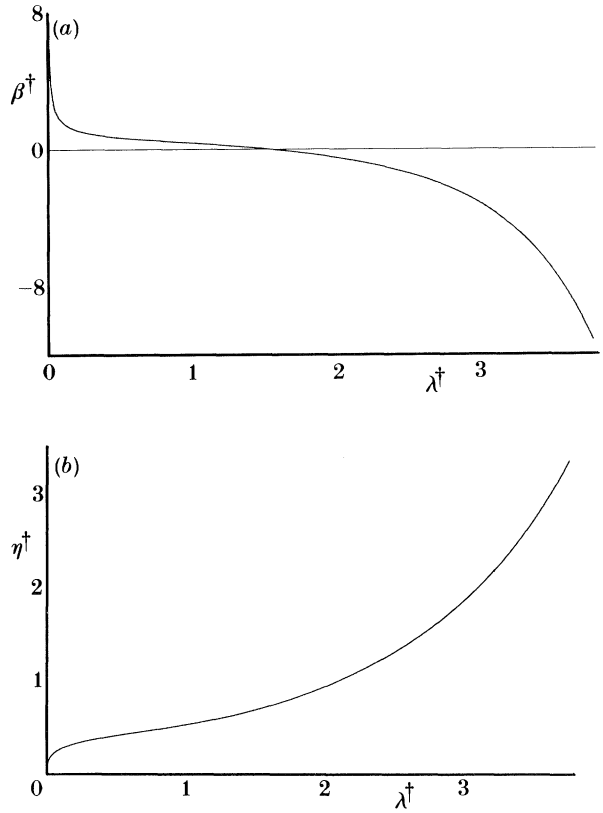

Figure 9. (*a*) The dependence of $\beta^\dagger$ on $\lambda^\dagger$. (*b*) The dependence of $\eta^\dagger$ on $\lambda^\dagger$.

The above discussion suggests that the most amplified wave for $G \gg 1$ is to be found where $k \ll G^{\frac{1}{4}}$. Suppose then that in order to find out the precise location of this mode we investigate the region $G \gg 1, k = O(1)$. In fact here the vortices satisfy the inviscid form of the vortex equations and have growth rates $O(G^{\frac{1}{2}})$. We are unaware of any previous work on the spatial modes of the inviscid Görtler problem so we give slightly more detail now than was given for the $k \sim G^{\frac{1}{4}}$ problem. The temporal inviscid Görtler problem is virtually identical to the inviscid Taylor problem and is set as an exercise by Drazin & Reid (1979), and discussed by Floryan (1986). Now let us look at the structure of the spatial inviscid Görtler modes and see if they include the fastest growing mode. We first expand u in the form

$$u = \exp\left[G^{\frac{1}{2}}\int \beta \,\mathrm{d}x\right]\{u_0(x,y) + G^{-\frac{1}{2}}u_1(x,y) + \ldots\}$$

together with a similar expansion for $G^{-\frac{1}{2}}v$. The eigenvalue problem for the amplification rate β is then found to be

$$-\beta^2\bar{u}[(\partial_y^2 - k^2)\,v_0 - (\bar{u}_{yy}/\bar{u})\,v_0] = k^2\chi\bar{u}_y\,v_0, \quad v_0 = 0, \quad y = 0, \infty. \tag{5.8}$$

Notice that since (5.8) corresponds to the inviscid limit we cannot satisfy the viscous boundary condition $v_{0_y} = 0$. For a given value of x we can solve (5.8) for the unstable eigenvalues, corresponding to $\beta > 0$. In particular, we note that (5.8) has the exact solution

$$v_0 = \bar{u}\exp(-ky), \quad \beta^2 = \tfrac{1}{2}k\chi, \tag{5.9a}$$

valid for all k. We note that for $k \ll 1$ there is a family of unstable modes with $\beta \sim k^{\frac{1}{2}}$; these modes are first significantly altered by viscous effects when $k \sim G^{-\frac{1}{7}}$ and become non-parallel when $k \sim G^{-\frac{1}{2}}$.

The above exact solution is valid only if $\bar{u}$ does not vanish in $(0, \infty)$ and corresponds to an unstable mode if χ is positive so that the wall is concave. Our primary concern in this paper is with the receptivity problem for a Blasius boundary layer but we shall now make a few remarks about the relevance of the above solution to other flows.

First, we note that a second exact solution of the differential equation for v_0 is

$$v_0 = \bar{u} \exp(ky), \quad \beta^2 = -\tfrac{1}{2}k\chi, \tag{5.9b}$$

but this solution does not satisfy the required boundary condition at infinity unless $\bar{u}$ vanishes there. More precisely we require that $\bar{u}$ goes to zero more quickly than does e^{ky}. Thus the second exact solution is relevant to for example wall-jet flows and corresponds to an unstable disturbance if χ is negative so that the wall has convex curvature. Hence a wall-jet flow is unstable in the presence of either convex or concave curvature. However, the magnitude of the growth rate depends only on the magnitude of the curvature, whilst the form of the eigenfunction depends only on the sign of the curvature. We further note that the second exact solution is also valid only for flows which do not have a change of sign in $\bar{u}$ within the flowfield. As one would anticipate the unstable modes for a flow having a change of sign of $\bar{u}$ are more complicated; in fact, they have a critical layer structure where $\bar{u}$ vanishes and viscous effects must be retained to remove the singularity in the disturbance velocity field. In that case the exact solutions describe the disturbance only in the region above the critical layer furthest from the wall. We note here that the eigenvalue of the unstable mode associated with such flows is still as given by (5.9*a*, *b*) dependent on the sign of the curvature. A result which is even more surprising is that (5.9*a*, *b*) apply to compressible boundary layers for which $\bar{u}$ does not change sign. Hence for a compressible boundary layer the temperature profile and Mach number no direct effect on the growth rate of what is in fact the most unstable inviscid mode. In fact the exact solution is only the first mode in an infinite hierarchy of modes which yield unstable eigenvalues if $\bar{u}_y$ is anywhere positive. However, we were unable to determine exact solutions of (5.8) for these higher modes. In figure 10 we present the first two unstable eigenvalues of (5.8); we have restricted attention to the Blasius flow and have, for convenience, chosen $x = \frac{1}{2}$. From (5.8) we expect that for small k the higher modes have unstable eigenvalues $\beta \sim k$. This prediction is born out by the results shown in figure 10 for the second mode.

We see from figure 10 that there is not a fastest growing mode predicted by our calculations since for the two modes calculated β tends to infinity when $k \to \infty$. In fact it is crucial to find this large k structure since it provides the vital clue in the search for the most unstable mode. The calculations we performed to construct figure 10 showed that the eigenfunction of any mode becomes concentrated at the wall as $k \to \infty$. This suggests that a new structure will emerge from (5.8) when $\partial/\partial y \sim k$ in which case there is a wall layer of depth k^{-1} near $y = 0$. Since $\bar{u} \sim y$ for y small it is clear that such a structure can exist only if $\beta \sim k^{\frac{1}{3}}$. We therefore write

$$\psi = ky, \quad \beta = \beta^{\dagger} k^{\frac{1}{3}}$$

and the reduced problem for $\beta^{\dagger}$ is then

$$-\beta^{\dagger 2}\{\partial^2 v_0/\partial\psi^2 - v_0\} = \chi v_0/\psi, \quad v_0 = 0, \quad \psi = 0, \infty.$$

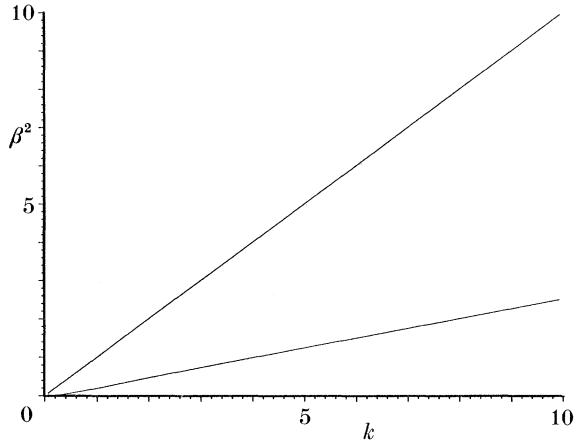

Figure 10. The dependence of the first two unstable eigenvalues β of (5.8) on k. Plotted is β^2 against k.

This is a form of Whittaker's equation

$$W''+[-\tfrac{1}{4}+K/z+(\tfrac{1}{4}-\mu^2)/z^2]\,W=0. \tag{5.10}$$

The solutions of this equation using the notation of Abramowitz & Stegun (1965) are $M_{K,\mu}(z)$, $W_{K,\mu}(z)$ and can be expressed in terms of Kummer functions. The above equation reduces to (5.10) if $\mu=\pm\frac{1}{2}$ and $2\beta^{\dagger 2}/\chi=1/K$.

We can infer from the small and large z forms of M, W given by Abramowitz & Stegun that if we are restricted to $\mu=\pm\frac{1}{2}$ then the only values of K which enable W to vanish at $z=0,\infty$ are $K=1,2,3\ldots$. Thus the unstable values of $\beta^\dagger$ are given by

$$\sqrt{2}\beta^\dagger=\chi^{\frac{1}{2}},\quad \chi^{\frac{1}{2}}/\sqrt{2},\quad \chi^{\frac{1}{2}}/\sqrt{3}\ldots.$$

Note here that the first eigenvalue is the exact solution valid for all k. Thus in the high wavenumber limit the inviscid modes become progressively more unstable with growth rate $\sim G^{\frac{1}{2}}k^{\frac{1}{2}}$. On the other hand we see that the viscous right-hand branch modes become more unstable as k decreases, actually from (5.1), (5.2) and (5.6c) we see that in that régime the growth rate is $\sim G^{\frac{1}{2}}(k/G^{\frac{1}{4}})^{-2}$. This suggests that the viscous and inviscid modes in these limiting cases will merge when $k\sim G^{\frac{1}{5}}$ since they will both then predict growth orders $\sim G^{\frac{3}{5}}$. Moreover, both limiting forms then suggest that the vortices will then be confined to a layer of thickness $G^{\frac{1}{5}}$ at the wall. Thus in this 'overlap régime' we write

$$k=\bar{\lambda}G^{\frac{1}{5}},\quad \Psi=ky,$$

and expand u in the form

$$u=\exp\left[G^{\frac{3}{5}}\int\beta(x)\,\mathrm{d}x\right]\{u_0+G^{-\frac{1}{5}}u_1+\ldots\}$$

together with a similar expansion for $G^{\frac{2}{5}}v$. Near the wall the basic flow $\bar{u}\sim\mu(x)\,y$ and the function pair (u_0,v_0) is found to satisfy

$$\left.\begin{aligned}\left\{\frac{\mathrm{d}^2}{\mathrm{d}\Psi^2}-\frac{\mu\beta\Psi}{\bar{\lambda}^3}-1\right\}u_0&=\frac{\mu}{\bar{\lambda}^2}v_0,\\ \left\{\frac{\mathrm{d}^2}{\mathrm{d}\Psi^2}-\frac{\mu\beta\Psi}{\bar{\lambda}^3}-1\right\}\left\{\frac{\mathrm{d}^2}{\mathrm{d}\Psi^2}-1\right\}v_0&=-\frac{\chi\mu\Psi u_0}{\bar{\lambda}^3},\\ u_0=v_0=v_0'=0,\quad \Psi&=0,\infty.\end{aligned}\right\} \tag{5.11}$$

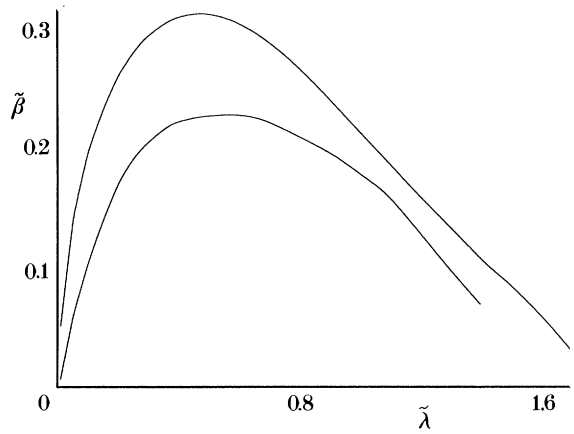

Figure 11. The dependence of the eigenvalue $\tilde{\beta}$ of (5.14) on $\tilde{\lambda}$.

The limiting inviscid form is then obtained from (5.11) by taking the further limit $\bar{\lambda} \to 0$ in (5.11), whilst the limiting form (5.6) is recovered by allowing $\bar{\lambda} \to \infty$ in (5.11). Thus without further calculation we know that the eigenvalues of (5.11) are such that

$$\beta \sim \bar{\lambda}^{\frac{1}{2}}, \quad \bar{\lambda} \to 0, \quad \beta \sim \bar{\lambda}^{-2}, \quad \bar{\lambda} \to \infty, \tag{5.12}$$

so that at some intermediate value of $\bar{\lambda}$ a most amplified case will exist. To confirm this we solved (5.11) numerically to obtain the first few unstable eigenvalues as functions of $\bar{\lambda}$. For computational purposes it is convenient to eliminate the parameters μ, χ from (5.11) by writing

$$\bar{\lambda} = (\chi\mu^2)^{\frac{1}{5}}\tilde{\lambda}, \quad \beta = (\chi^3\mu)^{\frac{1}{5}}\tilde{\beta}, \quad u_0 = \mu\tilde{u}_0, \quad v_0 = (\chi\mu^2)^{\frac{2}{5}}\tilde{v}_0 \tag{5.13a–d}$$

in which case (5.11) may be rewritten as

$$\left.\begin{aligned} \left\{\frac{\mathrm{d}^2}{\mathrm{d}\Psi^2} - \frac{\Psi}{\tilde{\lambda}^3}\tilde{\beta} - 1\right\}\left\{\frac{\mathrm{d}^2}{\mathrm{d}\Psi^2} - 1\right\}\tilde{v}_0 &= -\frac{\Psi\tilde{u}_0}{\tilde{\lambda}^3}, \\ \left\{\frac{\mathrm{d}^2}{\mathrm{d}\Psi^2} - \frac{\Psi}{\tilde{\lambda}^3}\tilde{\beta} - 1\right\}\tilde{u}_0 &= \frac{\tilde{v}_0}{\tilde{\lambda}^2}, \\ \tilde{u}_0 = \tilde{v}_0 = \tilde{v}_0' = 0, \quad \Psi &= 0, \infty. \end{aligned}\right\} \tag{5.14}$$

Thus (5.14) now constitutes an eigenvalue problem $\tilde{\beta} = \tilde{\beta}(\tilde{\lambda})$ and the first two unstable eigenvalues are shown in figure 11; we see that (5.12) is confirmed and that each unstable mode has its growth rate maximized at a finite value of $\bar{\lambda}$. Our calculations showed that the most unstable mode corresponds to $\tilde{\lambda} = \lambda_c = 0.476, \tilde{\beta} = 0.312$. Actually, in addition to the modes shown there is an infinite sequence of less unstable modes with a similar $\tilde{\beta}-\tilde{\lambda}$ structure moved progressively closer to the $\tilde{\lambda}$ axis.

Thus the above calculation has shown that the most unstable linear Görtler vortex at high Görtler numbers is viscous but with wavenumber $\sim G^{\frac{1}{5}}$ rather than $\sim G^{\frac{1}{4}}$ as would be appropriate to the unstable modes close to the neutral curve. A further significant result is that the most unstable vortices are close to the wall; this leads us to expect that, when the appropriate receptivity problem for these modes is discussed, $O(1)$ 'coupling coefficients' are possible. This problem is addressed in the next section; to close this section we make a few remarks about the nature of the

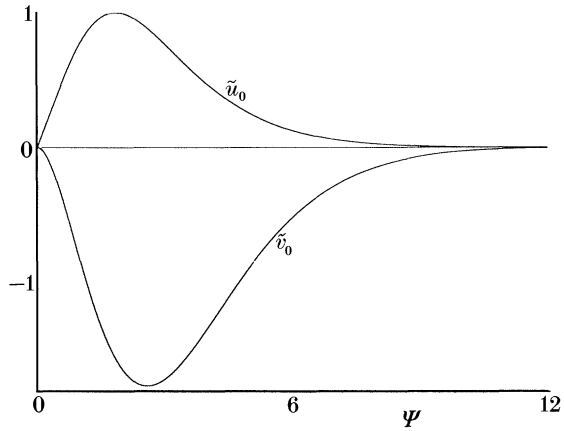

Figure 12. The velocity fields $\tilde{u}_0, \tilde{v}_0$ corresponding to the greatest eigenvalue of (5.14).

eigenfunctions associated with the most dangerous mode we have isolated. The $\tilde{u}_0$, $\tilde{v}_0$ velocity fields of the most dangerous mode are shown in figure 12. We see that they have the characteristic shape of vortices measured experimentally. In fact figure 13 shows a comparison of this most unstable eigenfunction with that measured by Swearingen & Blackwelder (1987). Also shown is the eigenfunction from Smith's (1955) parallel flow theory. We see that the predicted velocity field is close to that measured experimentally.

Now let us consider the evolution of a fixed wavelength vortex as it develops in the x direction. We note that it is observed experimentally that Görtler vortices develop such that their wavelength is conserved so $\bar{\lambda}$ = constant describes the experimental situation. For definiteness we suppose that the basic flow is a Blasius boundary layer so that

$$\mu = \tilde{\mu} x^{-\frac{1}{2}} = 0.4696 x^{-\frac{1}{2}}/\sqrt{2}$$

and further that the wall shape is such that

$$\chi \sim x^N, \quad \text{with} \quad N \text{ fixed}.$$

We can determine $\beta(\bar{\lambda})$ for such a situation by noting that

$$\beta = (x^{3N-\frac{1}{2}}\tilde{\mu})^{\frac{1}{5}}\tilde{\beta},$$

with

$$\tilde{\beta} = \tilde{\beta}(\tilde{\lambda}), \bar{\lambda} = \tilde{\lambda}\left(\frac{\tilde{\mu}^2}{x^{1-N}}\right)^{\frac{1}{5}}.$$

Experimentally it is observed that when a vortex develops downstream it conserves its wavelength. Thus for a given fixed value of N we compute $\tilde{\lambda} = \bar{\lambda}(x(1-N)/5)\,\tilde{\mu}^{-\frac{2}{5}}$ at the location x and read off the corresponding value of $\tilde{\beta}$ from figure 11. The growth rate β at that location is then computed from $\beta = (\tilde{\mu} x^{3N-\frac{1}{2}})^{\frac{1}{5}}\tilde{\beta}$. It follows that the maximum possible growth rate at any x will increase with x only if $N > \frac{1}{6}$. However we note that, in the special case $N = 1$, $\tilde{\lambda}$ is a constant so that the most unstable mode occurs at the same value of λ for all x and has magnitude increasing like $x^{\frac{1}{2}}$. This particular choice of $N = 1$ is significant for the asymptotic structure we have developed because in this case the local Görtler number varies like the fifth power of the local wavenumber so that only the magnitude of the maximum growth rate can depend on x. We note in passing that $N = \frac{1}{2}$ plays a similar role for neutral vortices corresponding to the right-hand branch of the neutral curve.

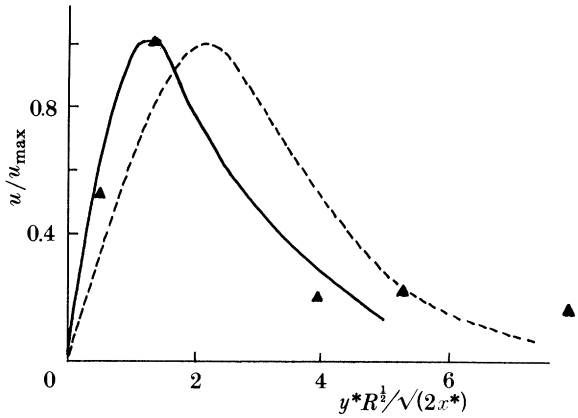

Figure 13. A comparison between the experimentally measured eigenfunction of Swearingen & Blackwelder (1987) and the corresponding eigenfunction calculated from the solution of (5.14). ▲, Experimental observation; ——, present calculation; – – –, Smith (1954).

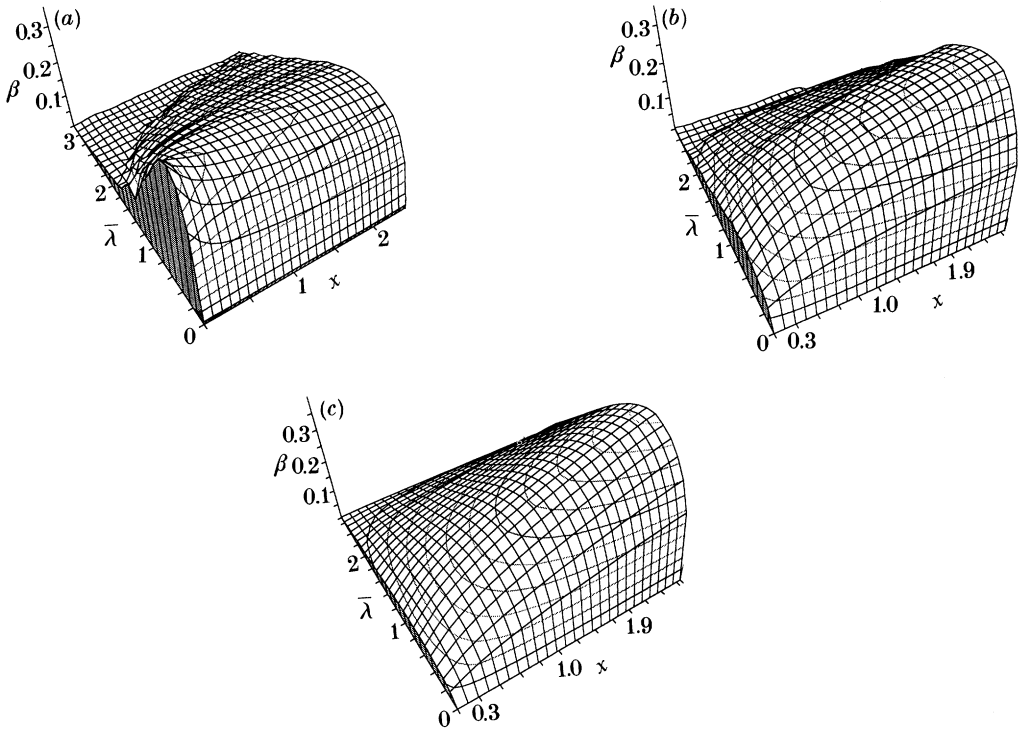

Figure 14. The dependence of β on λ and x for the cases (*a*) $N = 0$, (*b*) $N = \frac{3}{4}$ and (*c*) $N = 1$.

In fact if we do not take $N = 1$ we see that $\tilde{\lambda}$ either decreases or increases with x depending on whether $N > 1$ or $N < 1$. This means that for a given value of λ the growth rate $\beta(x)$ will have a maximum value at some value of x if $N \neq 1$. Thus if $N \neq 1$ there is a downstream location where a vortex of given wavelength is most amplified. In figure 14*a–c* we show β as a function of λ and x for the cases $N = 0, \frac{3}{4}$, 1. It should be noted that the development of a given vortex can be found from these figures by taking a slice through that figure parallel to the $\beta - x$ plane.

6. The receptivity problem for the most unstable Görtler mode

We have seen above that the crucial property of the most unstable vortex is that it is confined to a region of depth $G^{-\frac{1}{5}}$ near the wall. Suppose then that the wall forcing function $F(x)$ is of the form

$$\left.\begin{aligned} F &= 0, \quad x < \bar{x}, \\ F &= \tilde{F}(JG^{\frac{3}{5}}[x-\bar{x}]), \quad x \geqslant \bar{x}. \end{aligned}\right\} \tag{6.1}$$

Here we have introduced the factor $J = (\chi^3\mu)^{\frac{1}{5}}$ for convenience. Thus we are now allowing the wall forcing function to vary on a lengthscale comparable to the lengthscale over which the most unstable streamwise vortex develops. If we then define $\tilde{x}$ by

$$\tilde{x} = JG^{\frac{3}{5}}(x-\bar{x})$$

and write

$$\left.\begin{aligned} u &= u_0(\tilde{x}, \Psi) + G^{-\frac{1}{5}}u_1(\tilde{x}, \Psi) + \ldots, \\ (\chi\mu^2 G)^{-\frac{2}{5}}\mu v &= v_0(\tilde{x}, \Psi) + G^{-\frac{1}{5}}v_1(\tilde{x}, \Psi) + \ldots, \end{aligned}\right\} \tag{6.2}$$

then it follows directly from (5.14) that u_0, v_0 satisfy

$$\left.\begin{aligned} \left\{\frac{\partial^2}{\partial\Psi^2} - \frac{1}{\tilde{\lambda}^3}\Psi\frac{\partial}{\partial\tilde{x}} - 1\right\}u_0 &= \frac{1}{\tilde{\lambda}^2}v_0, \\ \left\{\frac{\partial^2}{\partial\Psi^2} - \frac{1}{\tilde{\lambda}^3}\Psi\frac{\partial}{\partial\tilde{x}} - 1\right\}\left\{\frac{\partial^2}{\partial\Psi^2} - 1\right\}v_0 &= -\frac{1}{\tilde{\lambda}^3}\Psi u_0. \end{aligned}\right\} \tag{6.3a, b}$$

Here $\tilde{\lambda}$, Ψ are as defined in the previous section. The forced problem then satisfies the conditions

$$\left.\begin{aligned} u_0 = \tilde{F}(\tilde{x}), \quad v_0 = 0, \quad \Psi = 0, \\ u_0, v_0 \to 0, \quad \Psi \to \infty. \end{aligned}\right\} \tag{6.4a, b}$$

In fact, we could modify the boundary condition as $\Psi \to \infty$ in order to allow for the possibility that vortices are induced by free-stream disturbances. However, since the disturbance in the free-stream must communicate with the wall layer over an $O(1)$ distance on a $G^{-\frac{1}{5}}$ lengthscale through a WKB structure similar to that of §3 the coupling coefficient for such a disturbance would be $O(\mathrm{e}^{-G^{-1/5}})$ and so this type of excitation will be weak compared to that discussed here. Alternatively we could investigate the effect of wall suction by setting $u_0 = 0$ at the wall and applying a non-zero boundary condition on v_0 there. The forced problem (6.3), (6.4) is most easily solved by again taking a Laplace transform with respect to the streamwise co-ordinate. If we denote the transforms of u_0, v_0, and $\tilde{F}$ by $\bar{u}_0, \bar{v}_0$ and $\bar{F}$, and assume that there is no incoming vortex field then we find that $\bar{u}_0, \bar{v}_0$ satisfy (5.14) with $\tilde{\beta}$ replaced by the transform variable s and the boundary conditions unchanged except for replacing the condition $\bar{u}_0 = 0, \Psi = 0$ by $\bar{u}_0 = \bar{F}(s), \Psi = 0$. We can write the solution of this problem in the form

$$(\bar{u}_0, \bar{v}_0) = \bar{F}(s)\,(u^*(s, \Psi), v^*(s, \Psi)), \tag{6.5}$$

where (u^*, v^*) satisfies the same problem as $(\bar{u}_0, \bar{v}_0)$ but with $\bar{F} = 1$. It is obvious at this stage that u^* and v^* will have singularities in the complex plane where $s = \tilde{\beta}_j$, the jth eigenvalue of (5.14) for $j = 1, 2 \ldots$. Moreover when we invert the transformed velocity field these singularities will in effect fix the form of the induced vortex field.

It is therefore essential that we should find the form of these singularities. We can obtain the form of (u^*, v^*) near the singularity by expanding (u^*, v^*) in the form

$$(u^*, v^*) = (u_0^*, v_0^*)/(s-\tilde{\beta}_j)+(u_1^*, v_1^*)+\dots. \tag{6.6}$$

If the above expansions are substituted into the differential system for (u^*, v^*) and s is replaced by

$$s = \tilde{\beta}_j+(s-\tilde{\beta}_j) \tag{6.7}$$

and terms of order $(s-\tilde{\beta}_j)^{-1}$ are equated in that system we obtain

$$(u_0^*, v_0^*) = \Delta_j(u_{0_j}(\tilde{\beta}_j, \Psi), v_{0_j}(\tilde{\beta}_j, \Psi)), \tag{6.8}$$

where Δ_j is a constant and (u_{0_j}, v_{0_j}) is the eigenfunction of (5.14) appropriate to $\tilde{\beta} = \tilde{\beta}_j$. At next order in the expansion procedure we find an inhomogeneous form of (5.14) to determine (u_1^*, v_1^*). If we define (b_j, f_j) to be the function pair adjoint to (u_{0_j}, v_{0_j}) then (b_j, f_j) satisfies

$$\left.\begin{aligned} \frac{\mathrm{d}^2 b_j}{\mathrm{d}\Psi^2}-\frac{\tilde{\beta}_j}{\tilde{\lambda}^3}\Psi b_j - b_j &= \frac{-\Psi}{\tilde{\lambda}^3} f_j, \\ \left(\frac{\mathrm{d}^2}{\mathrm{d}\Psi^2}-1\right)\left(\frac{\mathrm{d}^2}{\mathrm{d}\Psi^2}-\frac{\tilde{\beta}_j}{\tilde{\lambda}^3}\Psi-1\right) f_j &= \frac{b_j}{\tilde{\lambda}^2}, \\ b_j = f_j = f_j' = 0, \quad \Psi &= 0, \infty \end{aligned}\right\} \tag{6.9}$$

and the solvability condition for the system for (u_1^*, v_1^*) yields

$$\Delta_j = \bar{F} b_j'(0) \Big/ \int_0^\infty \{f_j\, \Psi(\mathrm{d}^2/\mathrm{d}\Psi^2-1)\, v_{0_j}/\lambda^3 + \Psi u_{0_j}/\lambda^3 b_j\}\, \mathrm{d}\Psi. \tag{6.10}$$

For convenience we assume at this stage that u_{0_j} has been normalized to have a maximum value of unity so that Δ_j is a measure of the transformed disturbance amplitude. It remains now for us to invert the transformed velocity field; in order to do so we must be more precise about the function $\bar{F}$. If we are interested in the effect of an isolated roughness element we can take F to be a function of compact support and then F cannot have any singularities in $s_r \geqslant 0$. If we wish to consider the effect of distributed roughness this restriction must be relaxed and we merely assume that $\bar{F}$ exists. In the first instance we assume that F has compact support then, since the only singularities of (5.10) in $s_r \geqslant 0$ correspond to the simple poles discussed above the contour of integration for the inverse transform is chosen parallel to the imaginary axis to the right of $s = \tilde{\beta}_1$. The contour is then closed in the left-hand half plane $\mathrm{Re}\,(s) < \tilde{\beta}_1$ and the only contributions to this integral come from the poles $s = \tilde{\beta}_j$. Thus we obtain

$$(u_0, v_0) = \sum_{j=1}^{\infty} (u_{0_j}, v_{0_j})\, \mathrm{e}^{\tilde{\beta}_j \tilde{x}} \Delta_j \bar{F}(\tilde{\beta}_j) \tag{6.11}$$

so that for a given value of $\bar{\lambda}$ the effective coupling coefficient is $\Delta_j \bar{F}(\tilde{\beta}_j)$ for the amplitude of the mode.

However, it is clear that for large x (6.11) will be dominated by the fastest growing mode which of course corresponds to $j = 1$. Thus when the Fourier transform is inverted to give the effect of a particular Z structure for the wall forcing by deforming the contour appropriately we will see that far downstream a vortex is set up with growth rate $\tilde{\beta}_1$ and with the wavelength $\bar{\lambda}$ corresponding to $\tilde{\beta}_1$. At this stage

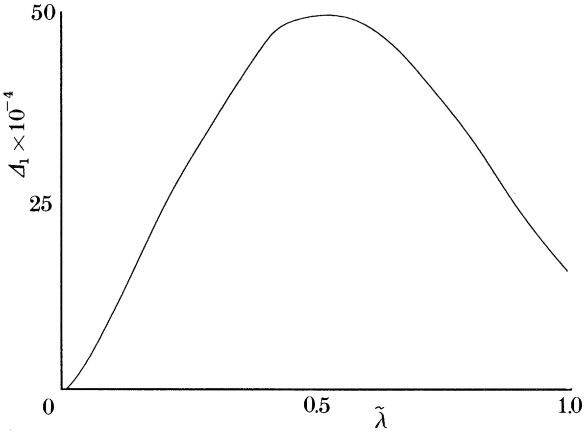

Figure 15. The 'amplitude' Δ_1 as a function of $\tilde{\lambda}$.

we could repeat the discussion of §4 and determine the effect of a three-dimensional obstacle on the onset of Görtler vortices. In fact the development of vortices in this region is essentially identical to that of §4. Thus behind a three-dimensional obstacle there will be a wake where initially the effect of the obstacle is concentrated; further downstream this wake will expand into a wedge-shaped region of vortex activity with a vortex wavelength corresponding to the most unstable mode of (5.10). The above discussion has assumed that F has compact support; if that is not the case then some further discussion is required. In fact if $\bar{F}$ does not have a pole to the right of $s = \tilde{\beta}_1$ then the large x downstream behaviour of the vortex flow will be as described above, since the associated velocity field will still be dominated by the pole at $s = \tilde{\beta}_1$. However, if $\bar{F}$ has a pole to the right of $s = \tilde{\beta}_1$ at, say, $s = s^*$ then F increases like $e^{s^* x}$ for large x and our original assumption that the wall perturbation is small becomes invalid. Thus the only situations described by our theory have the inverted velocity field dominated by the fastest growing mode of (5.10). Hence the question of whether the roughness element is isolated or distributed is not resolved for the fastest growing mode in either case. In either case $\bar{F}(\tilde{\beta}_1)$ will be an $O(1)$ number so that each type of forcing leads to an $O(1)$ coupling coefficient between the surface perturbation and the induced vortex field. In figure 15 we present a plot of Δ_1 against $\tilde{\lambda}$; we can see from this plot that Δ_1 attains its maximum at a finite value of $\tilde{\lambda}$. However, there is no reason to associate this value of $\tilde{\lambda}$ at which the maximum of Δ_1 occurs with that found in §5 for the most unstable vortex.

Finally in this situation we make a few remarks about more similarities between the solutions of (6.3) and those obtained in §4. First, we note that (6.3) has a small $\tilde{x}$ similarity solution essentially identical to that found in §4. Again the similarity variable is $\zeta = \Psi/\tilde{x}^{\frac{1}{3}}$ and for $\Psi = O(\tilde{x}^{\frac{1}{3}})$ it is easy to show that the solution expands as

$$u_0 = (1/\tilde{x})\,\bar{u}_0(\zeta) + \ldots; \quad v_0 = (1/\tilde{x}^{\frac{5}{3}})\,\bar{v}_0(\zeta) + \ldots,$$

with (u_0, v_0) given from a rescaled form of (4.3). Above this layer, where $\Psi = O(1)$, there is a region with $u_0 \sim (1/\tilde{x}^{\frac{4}{3}})\,\bar{\bar{u}}_0(y), v_0 \sim (1/\tilde{x}^{\frac{5}{3}})\,\bar{\bar{v}}_0(y)$ again, in fact it turns out that $\bar{\bar{v}}_0 \sim e^{-ky}$ there so that, if the z structure of the wall perturbation is concentrated near $z = 0$ and modelled by a delta function, above the $\tilde{x}^{\frac{1}{3}}$ layer the normal perturbation velocity in x, y, z space is proportional to $\tilde{x}^{-\frac{5}{3}} z/(y^2 + z^2)$. Note that in the wall layer the spanwise structure of the disturbance remains concentrated in a delta function form.

However, the similarity form $\sim z/(y^2+z^2)$ shows clearly the 'wake'-structure induced by a localized disturbance. This is precisely the situation observed in the numerical investigations of §4.

7. Conclusions

We shall, in the first place, draw some conclusions about the stimulation of Görtler vortices by wall roughness with spanwise wavelength comparable with the boundary-layer thickness. The key point in this situation is that Görtler vortices develop in a non-parallel manner; there is no such thing as a unique growth rate for a growing vortex or a unique neutral curve for a vortex which is not growing or decaying. Necessarily, this means that the receptivity problem for vortices of $O(1)$ wavelength must be dominated by non-parallel effects. In §4 we discussed the $O(1)$ wavelength receptivity problem for roughness elements varying in the streamwise direction on a lengthscale comparable with, and shorter than, the body scale. However, in the latter case our analysis fails if the roughness varies in the streamwise direction on the boundary layer lengthscale. We saw in §4 that, for a forcing function of the form (4.1) with F being a function with compact support, the effect of the forcing is to generate a similarity solution of the linear Görtler vortex equations in the neighbourhood of where the forcing occurs. By integrating the disturbance equations with the similarity solution used to generate the initial vortex field we were able to determine 'the' neutral curve appropriate to an isolated roughness element inserted into the boundary layer. Furthermore, we found that this type of forcing is a relatively inefficient generator of Görtler vortices because the vortex amplitude at the position where it begins to grow is an order of magnitude smaller than the amplitude of the forcing.

Where the forcing varies on the body lengthscale, the coupling coefficient is $O(1)$. In this case we found that behind a roughness element localized in the spanwise direction the disturbance initially decayed. Further downstream the disturbance was found to be 'reamplified' by centrifugal effects and a wedge of vortex activity generated. This pattern of vortex activity has been observed experimentally by, for example, Mangalam *et al.* (1991).

In §§3, 5 and 6 we concentrated on the case where the Görtler number is large and the vortex wavelength is small. The investigation of §4 showed conclusively that small wavelength vortices associated with the right-hand branch of the neutral curve suffer an exponential drop in amplitude because the region where they are unstable is an $O(1)$ distance from the region where the forcing occurs. Almost certainly this means that it is unlikely that small wavelength Görtler vortices could be produced by wall roughness in an experiment.

However, there is a situation when small wavelength Görtler vortices will be preferentially induced by wall roughness. We refer to the region discussed in §§5 and 6, where the vortex wavelength associated with the forcing is $O(G^{\frac{1}{5}})$. It is interesting to note that the fastest growing Görtler vortex described in §6 had not been identified by previous authors because it had been assumed that such a mode would have to be associated with disturbances close to the right-hand branch of the neutral curve. In fact, the fastest growing mode occurs in an overlap region between inviscid modes of wavenumber $O(1)$ and right-hand branch modes with wavenumber $O(G^{\frac{1}{4}})$. The eigenvalue problem (5.11), which determines the growth rate of the fastest growing mode, is, in fact, clearly related to the Taylor vortex problem for the flow

PHILOSOPHICAL TRANSACTIONS OF THE ROYAL SOCIETY A MATHEMATICAL, PHYSICAL & ENGINEERING SCIENCES

between concentric cylinders with the outer cylinder at rest and the inner cylinder rotating. In that case β corresponds to the azimuthal amplification rate of a steady, small wavelength Taylor vortex trapped near the outer cylinder. However, (5.11) has no neutral modes so that, for the Taylor problem, where the disturbance must be single valued in the azimuthal direction, this type of disturbance is not physically relevant. However, in other situations where no such constraint is appropriate (5.11) determines the fastest growing spatial mode of instability. Thus the eigenvalue problem (5.11) is directly relevant to the Taylor–Dean instability in pressure gradient driven flows in curved geometries, whilst a generalization of (5.11) involving a further second-order equation is relevant to the compressible Görtler problem with and without curvature. We see from (5.11) that the only dependence of the amplification rate on the mean state is through the wall shear μ, and in fact $\beta \sim \mu^{\frac{1}{5}}$. Thus the stabilizing effects of, for example, wall suction can be inferred directly from their effect on the wall shear.

Finally, we turn to the results we obtained in §6 for the receptivity problem associated with the fastest growing mode. Our main result in that section was that Δ_1, the coupling coefficient of the fastest mode, is an $O(1)$ quantity. This means that wall roughness at high Görtler numbers will stimulate vortices of wavenumber $G^{\frac{1}{5}}$ close to the position where the roughness begins. If the roughness is localized in the spanwise direction the vortex activity again begins in a wedge behind the obstacle. It remains an open question whether finite amplitude effects will significantly influence the structures we have discussed in this paper.

The authors acknowledge the support of SERC, ICASE and AFOSR for the research presented above. The authors also thank Helen Morris for pointing out a mistake in the original version of this paper and Dr A. P. Bassom for useful discussions. The authors are grateful for comments made by a referee.

References

Abramowitz, M. & Stegun, I. A. 1965 *A handbook of mathematical functions*. New York: Dover.

Cowley, S. & Hall, P. 1990 On the instability of the hypersonic flow past a wedge. *J. Fluid Mech.* **214**, 17.

Drazin, P. G. & Reid, W. H. 1979 *Hydrodynamic instability* (exercise 3.8). Cambridge University Press.

Floryan, J. M. 1986 Görtler instability of boundary layers over concave and convex walls. *Phys. Fluids* **29**, 2380.

Floryan, J. M. & Saric, W. S. 1979 Stability of Görtler vortices in boundary layers. *AIAA J.* **20**, 3, 316.

Hall, P. 1982*a* Taylor–Görtler vortices in fully developed or boundary layer flows: linear theory. *J. Fluid Mech.* **124**, 475.

Hall, P. 1982*b* On the nonlinear evolution of Görtler vortices in growing boundary layers. *J. Inst. Maths. Applic.* **29**, 173.

Hall, P. 1983 The linear development of Görtler vortices in growing boundary layers. *J. Fluid Mech.* **126**, 357.

Hall, P. 1988 The nonlinear development of Görtler vortices in growing boundary layers. *J. Fluid Mech.* **193**, 243.

Hall, P. 1990 Görtler vortices in growing boundary layers: the leading edge receptivity problem, linear growth and the nonlinear breakdown stage. *Mathematika* **37**, 151–189.

Hall, P. & Fu, Y. 1989 The Görtler vortex instability mechanism in hypersonic boundary layers. *J. theor. Comp. Fluid Mech.* **1**, 125–134.

Hall, P. & Fu, Y. 1990 The Görtler vortex instability in compressible boundary layers. In *Laminar–turbulent transition* (ed. D. Arnal & R. Michel). Springer-Verlag.

Hall, P. & Lakin, W. D. 1988 The fully nonlinear development of Görtler vortices. *Proc. R. Soc. Lond.* A **415**, 421.

Hall, P. & Malik, M. 1989 The growth of Görtler vortices in compressible boundary layers. *J. Engng Math.* **23**, 239.

Hall, P. & Seddougui, S. O. 1989 On the onset of three-dimensionality and time-dependence in the Görtler problem. *J. Fluid Mech.* **204**, 405.

Harvey, W. D. & Pride, J. D. 1982 The NASA Langley laminar flow control airfoil experiment. *AIAA paper* **82**-0567.

Hunt, J. C. R. 1971 A theory for the laminar wake of a two-dimensional body in a boundary layer. *J. Fluid Mech.* **49**, 159.

Mangalam, S. M., Dagenhart, J. R. & Meyers, J. F. 1991 Experimental studies on Görtler vortices. NASA Symposium on Natural Laminar Flow and Laminar Flow Control Research. *NASA TM* (In the press.)

Smith, A. M. O. 1955 On the growth of Taylor–Görtler vortices along highly concave walls. *Quart. Appl. Math.* **13**, 233.

Smith, F. T. 1973 Laminar flow over a small hump on a flat plate. *J. Fluid Mech.* **57**, 803.

Swearingen, J. D. & Blackwelder, R. F. 1987 The growth and breakdown of streamwise vortices in the presence of a wall. *J. Fluid Mech.* **182**, 255.

Wadey, P. 1990 Görtler vortex instabilities of incompressible and compressible boundary layers. Ph.D. thesis. Exeter University, U.K.

Received 9 May 1990; accepted 9 September 1990

PHILOSOPHICAL TRANSACTIONS OF THE ROYAL SOCIETY A MATHEMATICAL, PHYSICAL & ENGINEERING SCIENCES

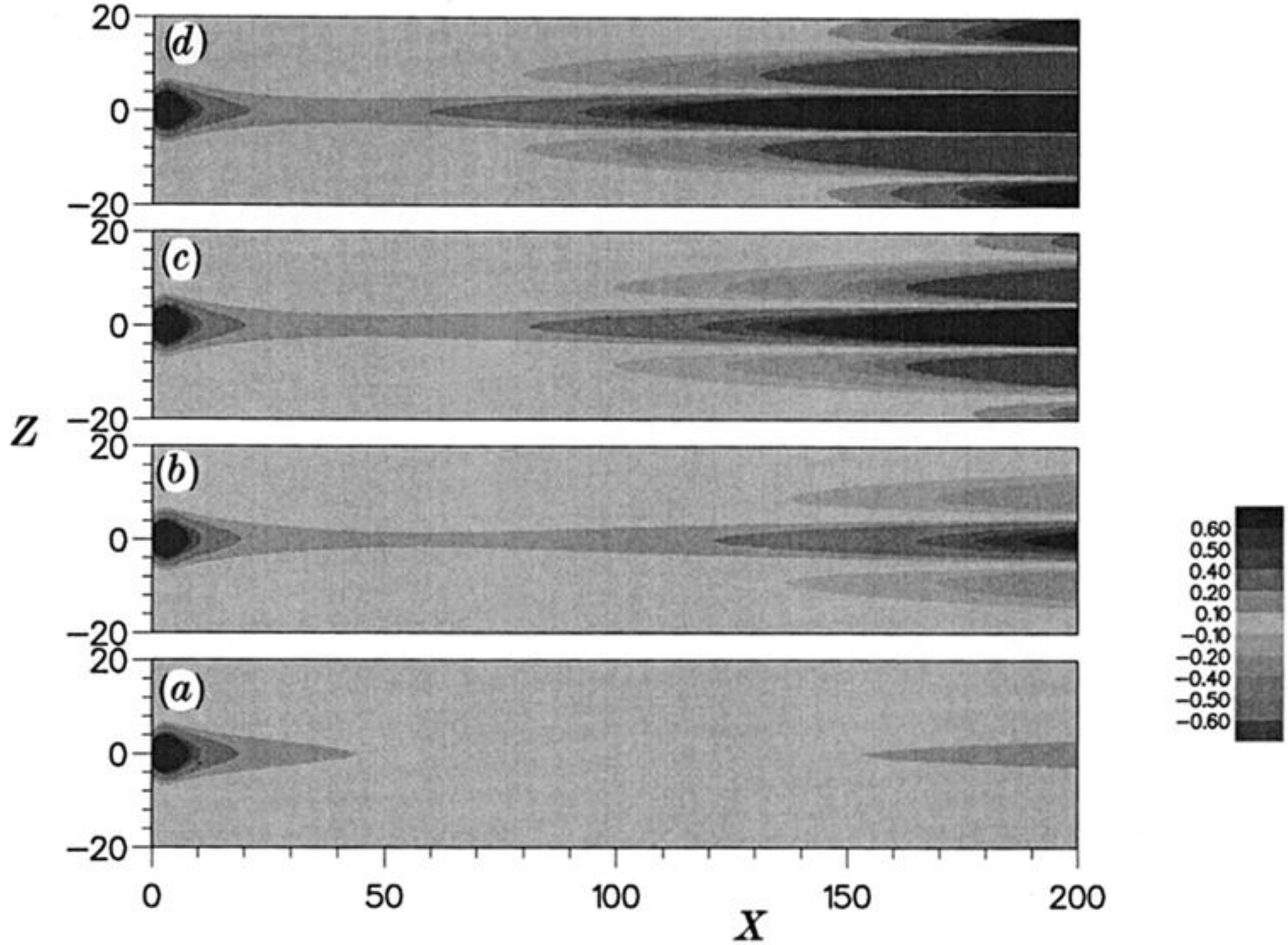

igure 7. Contour plots of u_m in the xz plane for the obstacle defined by (4.20). The results correspond to (*a*) $G = 4$, (*b*) $G = 8$, (*c*) $G = 12$ and (*d*) $G = 16$.

PHILOSOPHICAL TRANSACTIONS OF THE ROYAL SOCIETY A MATHEMATICAL, PHYSICAL & ENGINEERING SCIENCES

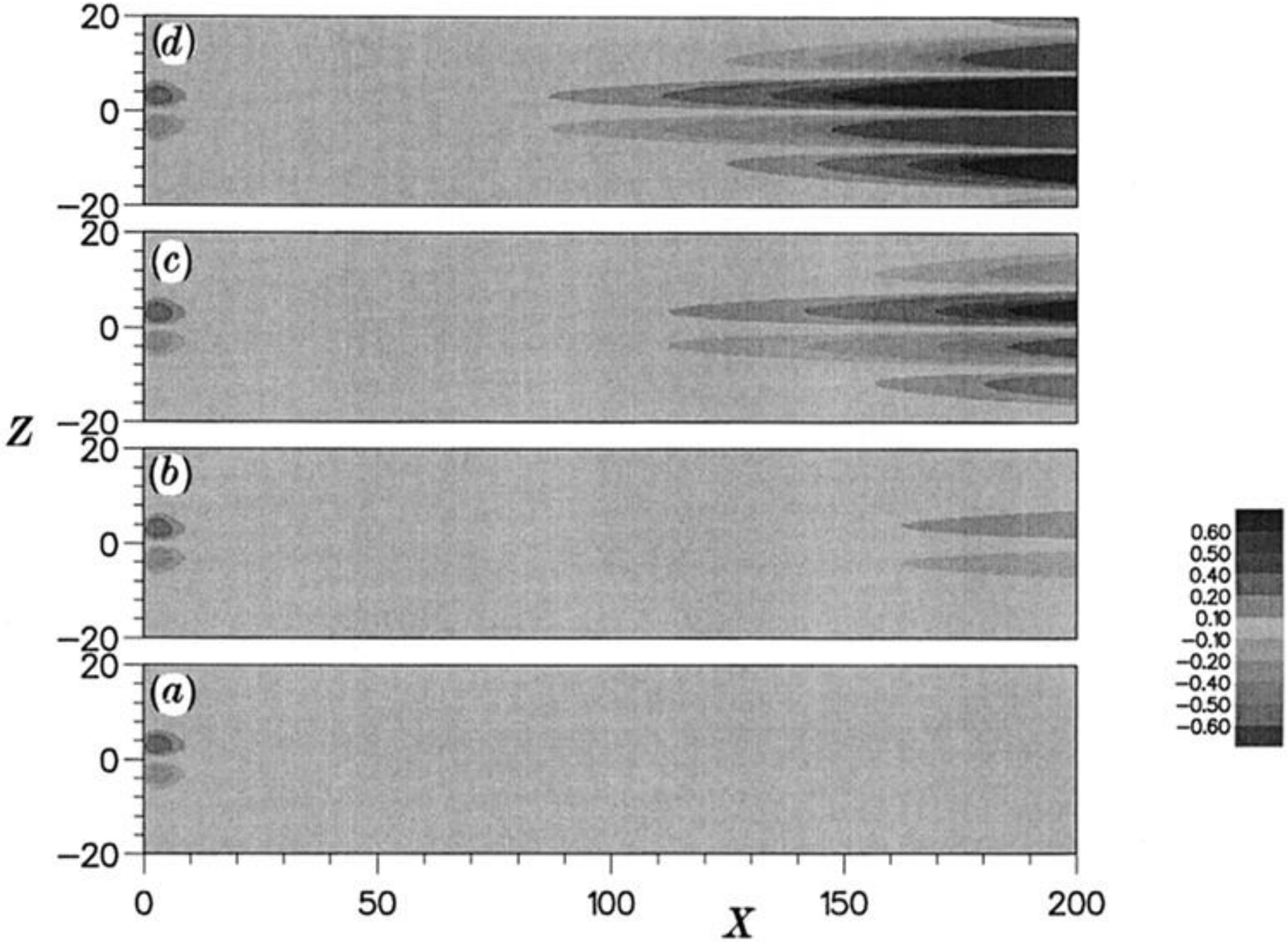

igure 8. Contour plots of u_m in the xz plane for the obstacle defined by (4.21). The results correspond to (*a*) $G = 4$, (*b*) $G = 8$, (*c*) $G = 12$ and (*d*) $G = 16$.

PHILOSOPHICAL TRANSACTIONS OF THE ROYAL SOCIETY A MATHEMATICAL, PHYSICAL & ENGINEERING SCIENCES